ON THE USE OF OPTIMIZED CUBIC SPLINE ATOMIC FORM FACTOR POTENTIALS FOR BAND STRUCTURE CALCULATIONS IN LAYERED SEMICONDUCTOR STRUCTURES

by

Kagiso Mpshe

Submitted in accordance with the requiements
for the degree of

MASTER OF SCIENCE

in the subject

PHYSICS

at the

UNIVERSITY OF SOUTH AFRICA

Supervisor: Prof. A. E. Botha

March 2015

Declaration

I declare that "*On the use of optimized cubic spline atomic form factor potentials for band structure calculations in layered semiconductor structures*" is my own work and that all sources that I have used or quoted have been indicated and acknowledged by means of references.

I further declare that I have not previously submitted this work, or part of it, for examination at Unisa for another qualification or at any other higher education institution.

Mr. K. Mpshe: _____

Date: _____

Acknowledgements

"*Learning is a treasure that will follow its owner everywhere.*"
Chinese Proverb

There are a number of people without whom this thesis might not have seen the light of day and to whom I am greatly indebted.

First of all, I would like to express my sincere gratitude to my MSc. supervisor Prof. André E. Botha for his constant guidance and patience throughout this work. Having worked with him has truly made me a better person in many ways.

I would like to thank Prof. Gaotsiwe J. Rampho and Prof. Mantile. L. Lekaka for their support and for providing counsel especially when the moral was low indeed they were my fortress. Many thanks to members of the physics department at the University of South Africa for their support and encouragement.

I wish to express my heartfelt gratitude to my family, especially my mother, Sibongile D. Mpshe and my late father Motsumi C. Mpshe for their consistent encouragement and unconditional love. I also wish to thank the mother of my new born son for her patience, unconditional love and understanding.-I hope to give you and our son enough attention before I begin my Ph.D studies in the next few months

The generous financial assistance from the University of South Africa's post graduate bursary and grow your own timber fund (GYOT) is highly appreciated. I also wish to thank Science Engineering and Information communication labs (SENDICT labs Pty Ltd) especially Mr. Gontse Mpshe who is the founder of the company for assisting me whenever necessary.

Most importantly I thank God the Almighty who continues to make the impossible possible - To God be all the Glory.

Summary

The emperical pseudopotential method in the large basis approach was used to calculate the electronic bandstructures of bulk semiconductor materials and layered semiconductor heterostructures. The crucial continuous atomic form factor potentials needed to carry out such calculations were determined by using Levenberg-Marquardt optimization in order to obtain optimal cubic spline interpolations of the potentials. The optimized potentials were not constrained by any particular functional form (such as a linear combination of Gaussians) and had better convergence properties for the optimization. It was demonstrated that the results obtained in this work could potentially lead to better agreement between calculated and empirically determined band gaps via optimization.

Keywords:

Emperical pseudopotential method, Large basis approach, Levernberg-Marquardt optimization, Cubic spline interpolation, Continuous atomic form factor potentials, Layered semiconductor structures, Energy bandstructure, Semiconductor heterostructures.

List of Figures

List of Tables

Contents

Chapter 1

Introduction

1.1 Background

Semiconductor materials continue to play an important role in the advancement of technological applications and therefore research on the properties of semiconductor structures has continued unabated. Historically in 1947, Bardeen and Brattain discovered the transistor effect while trying to understand the nature of the electrons at the interface between a metal and semiconductor. In 1956 Bardeen, Brattain and Shockley were awarded the Nobel Prize in physics, for research on semiconductors and their discovery of transistor effect[1]. Similar research also provided insight into other quantum effects in semiconductor materials; such as, tunneling phenomena in semiconductors (Nobel Price, 1973), electronic structure of magnetic and disordered systems (Nobel Price, 1977), the quantized Hall effect (Nobel Prize, 1985) and most recently graphene (Nobel Price, 2010)[2]. Semiconductors like silicon and germanium have been the cornerstone of the semiconductor industry since the early days, with silicon still being the key contributor in most electronic devices. However, due to its indirect band gap, silicon is unsuitable for certain opto-electronic applications, and therefore there is a need to design new materials to counter-act this short-fall [1]. Fortunately bandstructure theory, together with new

[1] See www.nobelprize.org/nobel_prizes/physics/laureates/1956 (last accessed 24/02/2015)

[2] www.nobelprize.org/nobel_prizes/physics/laureates (last accessed 24/02/2015)

computational and experimental techniques, affords us the opportunity to investigate the electronic structure of other materials which may also posses useful properties.

While early studies on semiconductors were based on bulk materials, resulting in the discovery of very useful properties, workers could not help but imagine combining bulk material to form so-called layered structures, or man-made materials. In the early 1970s Esaki and Tsu [2] succeed in developing the first kind of such a structure in the form of a superlattice. In their work they considered two experimental methods. In the first method a periodic variation of donor and acceptor impurities, was implanted in a single bulk semiconductor. In the second method they considered a periodic variation of alloy composition, introduced during the crystal growth [2]. The word superlattices means a periodic structure made of layers of two or more semiconductors deposited alternately on each other along the growth direction [2]. Typically the layer thicknesses are on the order of tens of nanometers, hence superlattices are also sometimes referred to nano-structures. Superlattices are related to quantum wells, since they are both composed of altinating layers of different semiconductor materials. They differ from quantum wells in that the layer thickness in superlattices is usually smaller leading to the dominance in the periodicity. In the case of quantum wells, the layers are usually thicker resulting in the dominance of the bulk properties of the individual layers. This essential difference will be elaborated upon in the next chapter.

1.2 Layout of dissertation

The layout of this dissertation is as follows. In the remainder of this chapter the rationale and objectives, advantages, and limitations of the present study are discussed. Chapter two provides a brief review of the relevant literature. In chapter three the main methods used in this work are explained. Chapter four discusses how we determine continuous atomic form factor potentials (CAFFPs) by using Levernberg-Marquardt optimization algorithm (LMA) in conjunction with cubic spline interpolation. In chapter five we provide the codes that were developed in this work, together with a description of how they work.

Chapter six presents our results and discussions of different bandstructures obtained. A summary of the main results and an outlook for the future work is provided in the concluding chapter.

1.3 Rationale and objectives

We consider the problem of calculating the electronic bandstructure of bulk semiconductor and layered semiconductor materials, within the frame work of emperical pseudopotential method and the large basis approach. The main focus of this work will be on obtaining the continuous atomic form factor potentials that are required to calculate the electronic bandstructure of superlattices and quantum wells. Electronic bandstructure is fundamentally important because it forms the foundation of any calculation of the transport properties of semiconductors.

For bulk materials the emperical pseudopotential method (EPM) can be used to compute the electronic bandstructure by knowing only the atomic form factors at discrete values of the magnitude of the reciprocal lattice vector $q = ||\mathbf{G} - \mathbf{G}'|| = 0, \sqrt{3}, \sqrt{4}, \sqrt{8}, \sqrt{11}$, where q has been expressed in units of $2\pi/a_0$, and a_0 is the lattice constant of the bulk material. However, in the case of layered structures, continuous atomic form factor potentials (CAFFPs) are required.

In the past, several interpolation schemes have been used to approximate the CAFFPs, $V(q)$ [3, 4, 5, 6, 7, 8, 9, 10, 11, 12]. Zunger *et al.* [3, 10, 11, 12] made use of a single Gaussian or a linear combination of four Gaussians to determine $V(q)$, with the Gaussian parameters fitted to reproduce certain key experimentally observed results, like the carrier effective mass and energy band gaps that can be deduces from optical spectra. Fridel *et al.* [6] fitted $V(q)$ by including a hyperbolic tangent term which was mainly used to truncate the pseudopotential at large q. Glembocki and Pollak [9], interpolated the local form factor for Germanium by following an approach due to Bednarek and Rösseler [13] in which they fitted to the Cohen and Bergstresser [14] form factors. Allen *et al.*

extrapolated $V(q=0) = -2E_F/3$, which is the values of the 'Heine-Abarenkov-Animalu model potential' [15], with E_F being the Fermi energy.

The purpose of the present work is to apply a least-square optimization technique, together with the cubic-spline interpolation, to develop an alternative scheme for interpolating the CAFFPs. Unlike previous work, which made use of linear combinations of Gaussian functions to interpolate the form factors, here we make use of optimized piecewise cubic spline interpolated atomic form factors which have better convergence properties than the Gaussians. As we will discuss in chapter four, the more rapid convergence properties of cubic spline is essential in order to perform the optimization calculation within a reasonable amount of time.

1.4 Advantages and limitations of the present study

Since it makes use of relatively small number of empirically fitted parameters, such as band gaps and effective masses, the emperical pseudopotential method (EPM) can be an extremely efficient method for calculating accurate electronic bandstructures. The EPM allows the form factor potentials to be adjusted in order to fit the experimental results. The EPM is well suited to full-zone bandstructure calculations and has already been widely applied in studies of semiconductors [1, 3, 4, 15, 16, 17]. However, the EPM is strictly speaking only applicable in the case of a single electron Schrödinger's equation, it does not explicitly take into account many body effects. Another limitation of this method is that the dimension N of the matrices that must be digonalized increases linearly with the superlattice period, i.e. Nn_z, where n_z is the superlattice period in units of the lattice constant a_0. This effectively makes it only possible to treat systems with layer thicknesses $\sim 10^2$ Å. Wang and Zunger [18] dealt with this limitation by developing the so-called 'folded-spectrum method', which allows calculations of eigenstates within a desired energy window. Other computational techniques, such as parallization, can also be employed to deal with the huge size of the matrices, if needed.

The existence of other theoretical frame works such as the $\mathbf{k}\cdot\mathbf{p}$ method [19, 20, 21] and density functional theory [22] offers workers the opportunity to share and compare data. These complementary approaches can also be used to probe the limitations of the EPM. Although mostly used for calculations at the zone centre, i.e. $\Gamma = 0$, the $\mathbf{k}\cdot\mathbf{p}$ can also be used over the full zone, provided a sufficient number of bands are included. Recently the $\mathbf{k}\cdot\mathbf{p}$ method has been applied in studies involving layered semiconductors. Wang *et al.* [23] used the $\mathbf{k}\cdot\mathbf{p}$ method to study the structure of abrupt $(\mathrm{InAs})_n/(\mathrm{GaSb})_n$ superlattices. Stier *et al.* [24] applied an 8-band $\mathbf{k}\cdot\mathbf{p}$ model to investigate the electronic and optical properties of strained quantum dots. Botha and Singh [25] studied the interaction between bulk and structural inversion asymmetry in the type-II quantum wells by employing a 14 band $\mathbf{k}\cdot\mathbf{p}$ model.

More recently Radhia *et al.* [26] extended the 15×15 $\mathbf{k}\cdot\mathbf{p}$ Hamiltonian derived by Cardona and Pollak [27], by adding spin-orbit coupling to the model; hence doubling the number of bands to give a 30×30 $\mathbf{k}\cdot\mathbf{p}$ Hamiltonian which they then employed to calculate the bandstructure of several direct band-gap semiconductors (InAs, InP, InSb). A 40-band $\mathbf{k}\cdot\mathbf{p}$ model was also used by Saïdi *et al.* [28] to fit the standard $\mathbf{k}\cdot\mathbf{p}$ band parameters at Γ, X and L valley indirect-band gap bulk material for the T_d group semiconductor. The $\mathbf{k}\cdot\mathbf{p}$ method is not computationally expensive since the size of the Hamiltonian matrix, which depends on the number of the bands used, is relatively small. One advantages of the $\mathbf{k}\cdot\mathbf{p}$ approaches is that it rely on relatively small number of input parameters, such as the momentum matrix elements and zone center band energies, which are precisely known.

The inability of the EPM to accurately account for the many-electron effects prompted the development of Density Functional Theory (DFT). A clear difference between DFT and the EPM is that DFT is an *ab-initio* approach which does not make use of any experimentally measured inputs. In the DFT approach an hypothesis on the geometric structure of the system is all that is needed to build the Hamiltonian operator [29]. One of the major draw-backs of DFT is the underestimation of the fundamental band gaps in bandstructure calculations [30, 31, 32, 33, 34, 35, 36]. In a paper by Perdew [36] it is argued that the underestimations of the gap in semiconductors and insulators is due to the

exchange correlation energy in the Kohn-Sham DFT. The need for an energy-depended potential which lie beyond the Kohn-Sham formalism is emphasized [36].

Hybertsen and Louice [31, 32] produced good results which agree well with experimental data for the band gap, optical transitions, and the band dispersions for silicon and diamond. Their theory is based on evaluation of $\sum(\mathbf{r}, \mathbf{r}', E)$ to first oder in the dressed Green's function and the screened coulomb interaction: the GW approximation. The failures of DFT are not the breakdowns of the theory itself but are due to the current exchange-correlation functionals [35]. Godby *et at.* [33, 34] showed how the DFT exchange correlation potential $V_{XC}(\mathbf{r})$ of a semiconductor is calculated from the self-energy operator $\sum(\mathbf{r}, \mathbf{r}', E)$, and how $\sum$ is obtained using the Green's function and the screen coulomb interaction (GW) approximation. In their work Godby *et al.* [33, 34], achieved good agreement with experimental data for Si, GaAs, AlAs and diamond. Recently Sun *et al.* [37] implemented first-principles relativistic pseudopotential calculations within generalized gradient approximation (GGA) to investigate the structural and electronic properties of quaternary InAs/GaSb superlattices with an InSb or GaAs type of interface.

The results of the present cubic spline CAFFPs are compared to DFT in chapter six. The $\mathbf{k} \cdot \mathbf{p}$ theory and the DFT is not the focus of this work. The literature on these two theories is merely included to providing some insight into the limitations of the EPM . Of course, both the $\mathbf{k} \cdot \mathbf{p}$ and DFT also have their own limitations. In the next chapter we include a brief review of the later two techniques. Although they are not used in this work, both the $\mathbf{k} \cdot \mathbf{p}$ method and DFT have been used successfully for many years in studies of semiconductors and it is therefore worth being familiar with these two related techniques.

Chapter 2

Review of Layered Semiconductor Structures, the Empirical Pseudopotential and Related Methods

In band theory it is essential to have an accurate knowledge of what happens near top of the valence band and near the bottom of the conduction band for different semiconductor structure. It is within this range of energies, that most properties of semiconductor materials can be experimentally determined. For example, knowledge of the fundamental band gap, which is the energy gap between the lowest conduction band and the highest valence band, can provide understanding of many electronic properties of semiconductors. There are many theoretical techniques that can be used to calculate the electronic structure of semiconductor materials. These techniques can be divided into two categories. The first category consist of emperical methods [1, 3, 4, 14, 15, 16, 17]. The second category consist of *ab initio* methods, such as Density Functional Theory (DFT) [38, 39, 40, 22], such methods are very useful, but are not the focus of this work. In this chapter we will provide a brief introduction to layered semiconductor structures in general, as well as the most important techniques for calculating their electronic bandstructures.

2.1 A review of layered structures and their applications

The focus of this work is on bandstructure calculations for layered semiconductor structures, i.e. superlattices and quantum wells. These structures are also called two dimensional systems, because the quantum confinement of the carriers occurs in one dimension only thus leaving two degrees of freedom. Quantum wires and quantum dots on the other hand are referred to as one-dimensional and zero-dimensional systems respectively, for the same reason. Figure 2.1 displays three different types of superlattices, classified in terms of their band alignment. In type-I superlattices the narrower band gap of one material falls entirely within that of the wider band gap material. This is sometimes called a straddled band gap alignment. Type-II have a staggered band gap alignment, and in type III the band alignment is completely offset (mixed).

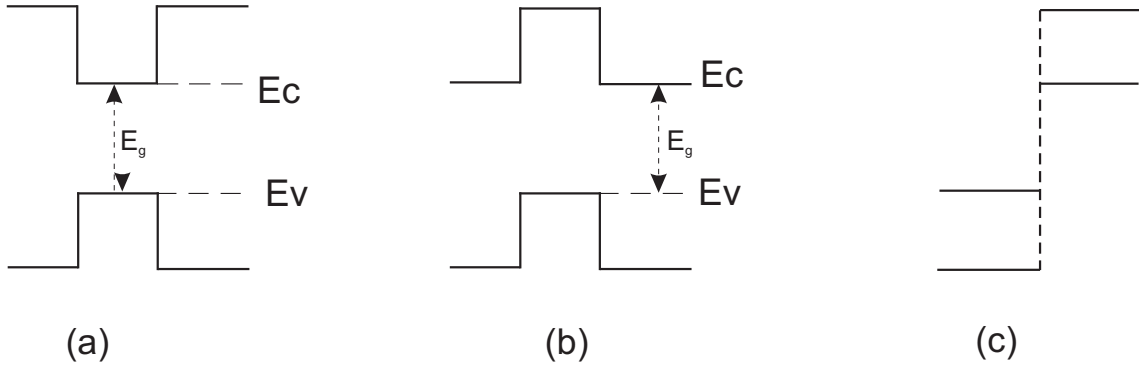

Figure 2.1: Classification of heterostructures according to band alignment: (a) straddled, (b) staggered, (c) mixed. E_C is the conduction band, E_V is the valence band and E_g is the band gap or energy gap.

There are two main growth techniques which are used to manufacture superlattices; molecular beam epitaxy and Metal organic vapor deposition [41]. Superlattices still have a wide range of potential applications such as long-wave optical sources, signal processing devices and mid-infrared detectors, therefore there is always a need to continue research in this field. In recent times a large amount of research has been done on all types of superlattices

and many applications exist. This research is primarily prompted by their opto-electronic transport properties. InAs and GaSb are direct band gap materials and combining these two semiconductors can offer many interesting properties which can be directly applicable in our every day lives. For short lattice periods the InAs/GaSb superlattices, and with a deliberate addition of strain these superlattices exhibit interesting properties which might be of great use in the development of the infrared detectors which have got a relevant application mostly in the military [42, 43, 44]. Third generation infrared photon detectors provide too advanced capabilities like better resolution, high pixels and multicolor functionality [43]. It has been discovered that the type-II superlattice can also provide an alternative to the photo-diodes, and also provide a solution to the long wave infrared region, since mercury cadmium telluride (HgCdTe) fail to give the requirements of large format two-dimensional arrays due to the problems of epitaxial layers such as uniformity and number of defective elements [43].

Yao [45] studied the thermal properties of semiconductor superlattices for the first time. In his work he measured the thermal diffusivity and thermal conductivity of the AlAs/GaAs superlattices. Yao [45] found that the thermal diffusivity and thermal conductivity decreases with a decrease in superlattice period. Sai-Halasz *et al.* [46] showed that under certain conditions like layer thickness, superlattices have a tendency of changing from semiconductor to semi-metal and also to metal. Superlattices consisting of alternating layers of extremely thin films often demonstrate strong quantum size effects that have been utilized to improve conventional devices and develop new ones [47]. Indeed superlattices have a wide range of applications and therefore research in semiconductor superlattices needs to be continued. In this work we study the AlAs/GaAs superlattices by making use of the emperical pseudopotential method (EPM) in the large basis approach.

2.2 A brief review of the emperical pseudopotential method applied to superlattice structure

The empirical methods are methods which make use of experimentally fitted parameters such as the band gap, lattice constant etc. In these kinds of approaches the electronic structure of the constituent materials is assumed to be understood and to be described by a parameterized bulk model [48]. The parameters of the bulk model are assumed not to change when the constituent materials are combined to form a superlattices [48]. The method adopted in this work is the one which makes use of empirically fitted parameters.

Almost a decade after Eskai and Tsu [2] developed the first superlattice, Caruthers and Lin-Chun [49, 50] reported for the first time the application the emperical pseudopotential method to superlattice heterostructures. In their work they calculated the electronic structure of the GaAs-$Ga_{1-x}Al_xAs$ repeated mono-layer heterostructure. Andreoni and Car [51] made use of the pseudopotential method to calculate the energy band structure of the $(GaAs)_n/(AlAs)_m$. The strength and the reliability of the EPM for electronic structure calculations of different heterostructures has been shown over the years. In the early 1990's Gell applied the EPM to calculate the valence-band effective masses in strained Si/Ge semiconductor structure by taking in to account the effect of the spin orbit couplings.

The effects of the spin orbit couplings in electronic structure calculations is well explained in a paper by Dresselhaus [52]. Mäder and Zunger [3] applied the EPM to a large scale electronic structure calculations by investigating the AlAs/GaAs superlattices. Subsequently Chen *et al.* [53] made use of the EPM to calculate the band structure of a coherently strained Si layer on GaAs. We make use of the empirical pseudopotential method (EPM) in the large basis approach to calculate the bandstructure of layered semiconductors. This method is explained in detail in chapter three.

2.3 A brief review of the multiband $\mathbf{k} \cdot \mathbf{p}$ method

The method was developed by Kane [19, 20] in the early days of semiconductor physics and since its introduction this method has been frequently used in the study of electronic properties of semiconductor structures. The $\mathbf{k} \cdot \mathbf{p}$ method can be used to find analytic expressions for band dispersion and effective masses. In most cases the $\mathbf{k} \cdot \mathbf{p}$ method is usually used to describe the band structure close to the zone center i.e. at $\mathbf{k} = 0$ but it can also be used over a full zone provided a large enough basis is used.

This method is sometimes referred to as the multiband envelope function or the multiband effective mass method. This is because of the fact that Hamiltonian which describe system are matrices, or systems of coupled Schrödingers equation, which gives the possible energies and wave functions expressed as a set of envelope functions [54]. The Hamiltonian is named after the number of bands that are explicitly included i.e. their wave functions are explicitly evaluated. The 4 and 6 band Hamiltonians for the valence envelope wave function were reported by Luttinger and Kohn [55]. Almost a decade later the 8-band model that included the conduction band was developed by Pidgeon and Brown [56]. Due to the fact that the model can use a relatively small number of bands, it can be consider as a simple but yet effective model.

In recent times this method has been used in the studies involving zincblende and layered semiconductor structures. The method has played an important role in providing the much needed theoretical insight responsible for the development of technology based on zincblende and layered semiconductor devices during the 1980's and 1990's [23, 57, 58]. For more details on this approach one can see Refs. [1, 19, 20, 59]

2.4 A brief review of density functional theory

The fundamental principle on which the Density Functional Theory is build upon is that any property of a system of many interacting particles can be viewed as a functional of

the ground state density $\rho(\mathbf{r_0})$ .i.e. one scalar function of a position $n(\mathbf{r})$, in principle determines all the information in the many body wavefunction for the ground state and all the exited states [60].

Thomas and Fermi first proposed the original density functional theory of quantum system in what is known as the Thomas-Fermi model [60]. In their method, they treated the kinetic energy of the system of electrons as an approximated explicit functional of of the density, idealized as non-interacting electrons in a homogeneous gas with the density equal to the local density at any given point. The limitations in the Thomas-Fermi model is due to the fact the exchange and the correlation amongst the electrons is not taken into account and this leads to the model not providing accurate desired results. While it is true that the Thomas-Fermi model does not give good enough results for the modern day calculation it has however laid proper foundation for improvements to be made [60], and indeed it was Dirac [39] who first made the much needed improvements by formulating the local approximations for the exchange and correlations.

The modern density functional theory formulation is due to Hohenberg and Kohn [40] who showed that a special role can be assigned to the density of particles in the ground state of a quantum many-body system i.e. all the properties of the system can be considered as to be unique functionals of the ground state density. In the following year in the paper by Kohn and Sham [22] major improvements on density functional theory were reported. The Kohn-Sham approach has led to very important approximations which provide the basis of most calculations which attempts to make the first principle or the *ab initio* predictions for the properties of condensed matter and molecular systems [60].

In the Kohn-Sham approach the original many-body problem is replaced with an independent electron problem that is easily solvable [60]. The Kohn-Sharm *ansatz* and its impact on the formulation and the calculations on density functional theory is well discussed in Ref. [60] and so here we will just give a brief discussion on that. Reliable and accurate results for wide bands semiconductor materials such as the group IV and II-V semiconductor materials can be obtained through the use of the local density approximation (LDA) and the generalized gradient approximation (GGA) [36]. The formulation of

the density functional theory is not considered a priority in this work since in any case it beyond the scope of our work, however interested readers are referred to Ref. [60] for more details on this method.

Chapter 3

The Empirical Pseudopotential Method

3.1 Introduction

This chapter provides a more detailed explanation of the emperical pseudopotential method (EPM), which is one of the main methods used in this dissertation. The material covered here follows closely that which is found in Refs. [15, 16, 54] The EPM method was developed in the early days of semiconductor physics and was originally introduced by Phillips and Kleinman [61, 62, 63] between the years 1958 and 1960. Since its introduction the EPM has become an important tool for electronic bandstructure studies of solids and for understanding the behavior of electrons in a crystal. In 1966 Cohen and Bergstresser [14] extended the model to include zinc blende semiconductors. Bloom and Bergstresser [64] went on to include the effects of spin-orbit coupling in their full-zone band structure calculations for α-Sn, InSb and CdTe. Their work was based on a modified model proposed by Weisz [65]. Based on the work by Bloom and Bergstresser [64], Walter and Cohen [66] calculated the bandstructures for ZnTe and ZnSe, including for the first time the spin-orbit interactions.

The aforementioned studies were all based on a simplified "local" approximation of the core potentials. However, later it was demonstrated through the X-ray Photoelectrons Spectroscopy (XPS) and Ultraviolet Photoelectrons Spectroscopy (UPS) data that local empirical pseudopotential calculations yielded incorrect values for the valence bands widths. The non-local EPM with spin-orbit coupling was developed by Chelikowsky and Cohen [17] and applied in their calculations of the full band structure for 11 zinc blende and diamond semiconductor structures. Their work produced excellent results which agreed well with the available experiments. The resulting bandstrucures obtained in Ref. [17] are still widely used and published in reference books, such as the well known Landolt-Börnstein tables [67]. Chelikowsky and Cohen [17] conducted a study of 11 diamond and zinc blende semiconductor structures, which included all of the materials studied previously. Following on these results the EPM has been extensively used by many groups [5, 6, 68, 69, 70, 71] to calculate the electronic band structure of relaxed or strained group-IV and III-V bulk semiconductor where the continuous atomic pseudopotential form factor $V(q)$ is a requirement [15]. The atomic form factor is the measure of the amplitude of the out going spherical wave relative to the outgoing plane wave.

The major advantage of the EPM is that while it requires only few adjustable parameters the bandstructure calculations can be done for a full k space representation. This allows comparison between the experimental data and theoretical data to be compared at high symmetry points along the k space such as the X, Γ, and L points. One disadvantage of the EPM is that it can be computationally expensive, particularly in large basis approaches. While the issue of memory allocation for storing a large Hamiltonian matrix is no longer a problem, thanks to modern technology, the issue filling and solving a large Hamiltonian matrix still remain. In the large basis approach the order of the Hamiltonian matrix increases linearly with the superlattice period .

3.2 Principles and approximations

To calculate the electronic structure of semiconductors we need to solve the Hamiltonian representing a complete crystal. Such a Hamiltonian $\mathcal{H}$ consist of the kinetic energies of

electrons and the cores, the core-core, electron-electron, and the electron-core Coulomb interactions and relativistic effects [16]. Thus $\mathcal{H}$ can be written as [54]

$$\mathcal{H} = \mathcal{H}_{electrons} + \mathcal{H}_{nuclei} + \mathcal{H}_{electrons-nuclei}, \tag{3.1}$$

where

$$\mathcal{H}_{electron} = \sum_{\mu} \left(-\frac{\hbar^2}{2m_0}\nabla_{\mu}^2 + \sum_{\lambda<\nu} \frac{e^2}{|\mathbf{r}_{\lambda} - \mathbf{r}_{\mu}|} \right), \tag{3.2}$$

$\mathbf{r}_{\mu}$ are the positions of the electrons, and m_o is the rest mass of the electron mass. The Hamiltonian due to the interaction of the nuclei is given by,

$$\mathcal{H}_{nuclie} = \sum_{\nu} \left(\frac{\hbar^2}{2M_{nu}}\nabla_{\nu}^2 + \sum_{\lambda<\nu} \frac{Z_{\lambda}Z_{\nu}e^2}{|\mathbf{R}_{\lambda} - \mathbf{R}_{\nu}|} \right) \tag{3.3}$$

where $\mathbf{R}_{\nu}$ are the positions of the nuclei, Z_{ν} are the atomic numbers and M_{ν} are the masses of the nuclei [54]. The Hamiltonian representing the interactions between the electrons and the nuclei is,

$$\mathcal{H}_{electron-nuclie} = -\sum_{\mu,\nu} \frac{Z_{\nu}e^2}{|\mathbf{R}_{\nu} - \mathbf{r}_{\nu}|}. \tag{3.4}$$

Taking into account that in a typical microscopic sample of a semiconducting crystal, there are a lot of nuclei, and correspondingly a lot of electrons, solving a Hamiltonian of such a system becomes a difficult problem. We therefore need to make assumptions and approximations in order to reduce the Hamiltonian (3.1) into a more manageable form. For the purpose of this work we just make assumptions without proves. By assuming that the electrons below the outer shell are tightly bound to the nucleus thus the atoms can be treated as separate entities and hence the number of particles is reduced [54]. The adiabatic (or Born-Oppenheimer approximation) assumes that electrons behaves adiabatically in the cores (i.e change in the coordinates of a nucleus passes no energy to the electrons, this then allows the decoupling of motions of the nuclei and the electrons [54]. The independent electron approximation removes the complications of the electron-electron interaction and replaces them with an average potential [54]. The mean field approximations considers only one at the time and assumes that each electron moves in the average field created by all the other electrons [15]. By making use of all these assumptions and approximations Eq. (3.1) reduces to a more manageable form:

$$\mathcal{H} \approx \frac{\hbar^2}{2m_o}\nabla^2 + V_c. \tag{3.5}$$

Equation (3.5) is the Hamiltonian for an electron of rest mass m_0, travelling in an effective crystal potential V_c. This crystal potential represents not only interaction between electrons and nuclei of atoms that constitute the lattice, but also the interaction between the electrons them selves.

3.3 Electronic bandstructure calculations

The objective of band theory for any model of a semiconductor material, is to determine the relationship between the energy E, and the crystal wave vector k. Bandstructure calculations are usually the first step in determining many of the microscopic properties of semiconductors. In calculating the bandstructure, we may start by determining the crystal potential V_c and then finding the solution of the Schrödinger's equation

$$\mathcal{H}\psi_{n,\mathbf{k}} = E_{n,\mathbf{k}}\psi_{n,\mathbf{k}}. \tag{3.6}$$

Since the crystal potential is periodic throughout, we employ the idea of Bloch, and expand the wave function $\psi_{n,\mathbf{r}}$ in Eq. (3.6) in terms of a complete orthonormal set of plane so that,

$$u_{\mathbf{G},\mathbf{k}} = \frac{1}{\sqrt{\Omega}} e^{i(\mathbf{G}+\mathbf{k})\cdot\mathbf{r}} \tag{3.7}$$

and then

$$\psi_{n,\mathbf{k}}(\mathbf{r}) = \sum_{\mathbf{G}} a_{n,\mathbf{k}}(\mathbf{G}) u_{\mathbf{G},\mathbf{k}} \tag{3.8}$$

and therefore

$$\psi_{n,\mathbf{k}}(\mathbf{r}) = \frac{1}{\sqrt{\Omega}} \sum_{\mathbf{G}} a_{n,\mathbf{k}}(\mathbf{G}) e^{i(\mathbf{G}+\mathbf{k})\cdot\mathbf{r}}. \tag{3.9}$$

Where $\psi_{n,\mathbf{k}}(\mathbf{r})$ is the wave vector, Ω is the total volume, $\mathbf{G}$ is reciprocal lattice vector and $\mathbf{k}$ is the electron momentum. Taking $\mathbf{R}$ to be the bravais lattice vector from Eq. (3.8) we have,

$$\psi_{n,\mathbf{k}}(\mathbf{r}+\mathbf{R}) = \frac{1}{\sqrt{\Omega}} \sum_{\mathbf{G}} a_{n,\mathbf{k}}(\mathbf{G}) e^{i(\mathbf{G}+\mathbf{k})\cdot(\mathbf{r}+\mathbf{R})} \tag{3.10}$$

which gives

$$\psi_{n,\mathbf{k}}(\mathbf{r}+\mathbf{R}) = \frac{1}{\sqrt{\Omega}} \sum_{\mathbf{G}} a_{n,\mathbf{k}}(\mathbf{G}) e^{i(\mathbf{G}+\mathbf{k})\cdot\mathbf{R}} e^{i(\mathbf{G}+\mathbf{k})\cdot\mathbf{r}} \tag{3.11}$$

and therefore

$$\psi_{n,\mathbf{k}}(\mathbf{r}+\mathbf{R}) = e^{i\mathbf{k}\cdot\mathbf{R}} \frac{1}{\sqrt{\Omega}} \sum_{\mathbf{G}} a_{n,\mathbf{k}}(\mathbf{G}) e^{i\mathbf{G}\cdot\mathbf{R}} e^{i(\mathbf{G}+\mathbf{k})\cdot\mathbf{r}} \tag{3.12}$$

which yield the Bloch's theorem

$$\psi_{n,\mathbf{k}}(\mathbf{r}+\mathbf{R}) = e^{i\mathbf{k}\cdot\mathbf{R}} \psi_{n,\mathbf{k}}(\mathbf{r}). \tag{3.13}$$

which is true provided that a set of wave vectors $\mathbf{G}$ can be found for the original expansion, which satisfy:

$$\mathbf{G}\cdot\mathbf{R} = 2\pi n, n \in Z. \tag{3.14}$$

Equation (3.14) is a set of vectors called reciprocal lattice vectors which describe the periodicity of the lattice. This set of vectors is indeed necessary for the implementation of the Bloch's Theorem and we proceed further to deduce the results. From the Schrödinger's equation Eq. (3.6) and the expansion of ψ Eq. (3.7) yields,

$$\mathcal{H} \sum_{\mathbf{G}} a_{n,\mathbf{k}}(\mathbf{G}) u_{\mathbf{G},\mathbf{k}} = E_{n,\mathbf{k}} \sum_{\mathbf{G}} a_{n,\mathbf{k}}(\mathbf{G}) u_{\mathbf{G},\mathbf{k}}. \tag{3.15}$$

By multiplying Eq. (3.15) from left to right by a plane wave $u^*_{\mathbf{G},\mathbf{k}}$ and integrating over all space we get,

$$\sum_{\mathbf{G}} a_{n,\mathbf{k}}(\mathbf{G}) \int u^*_{\mathbf{G},\mathbf{k}} \mathcal{H} u_{\mathbf{G},\mathbf{k}} d\tau = \sum_{\mathbf{G}} a_{n,\mathbf{k}}(\mathbf{G}) E_{n,,\mathbf{k}} \int u^*_{\mathbf{G},\mathbf{k}} u_{\mathbf{G},\mathbf{k}} d\tau \tag{3.16}$$

if we apply orthonomality property which states,

$$\int u^*_{\mathbf{G}',\mathbf{k}} u_{\mathbf{G},\mathbf{k}} d\tau = \delta_{\mathbf{G}',\mathbf{G}} \tag{3.17}$$

and writing

$$\mathcal{H}_{\mathbf{G}',\mathbf{G}} = \int u^*_{\mathbf{G}',\mathbf{k}} \mathcal{H} u_{\mathbf{G}',\mathbf{k}} \delta_{\mathbf{G}',\mathbf{G}} \tag{3.18}$$

then Eq. (3.16) reduces to

$$\sum_{\mathbf{G}} a_{n,\mathbf{k}}(\mathbf{G}) \mathcal{H}_{\mathbf{G}',\mathbf{G}} = \sum_{\mathbf{G}} a_{n,\mathbf{k}}(\mathbf{G}) E_{n,\mathbf{k}} \delta_{\mathbf{G}',\mathbf{G}}. \tag{3.19}$$

This equation is possible for each value of the electron wave vector **k**. From the one electron Hamiltonian Eq. (3.5) and Eq. (3.7) and also Eq. (3.18) the Hamiltonian can be expressed as,

$$\mathcal{H}_{\mathbf{G}',\mathbf{G}} = \frac{1}{\Omega}\int e^{-i(\mathbf{G}'+\mathbf{k})\cdot\mathbf{r}}\left(-\frac{\hbar^2}{2m_0}\nabla^2\right)e^{i(\mathbf{G}+\mathbf{k})\cdot\mathbf{r}}d\tau + \frac{1}{\Omega}\int e^{-i(\mathbf{G}'+\mathbf{k})\cdot\mathbf{r}}V_c e^{i(\mathbf{G}+\mathbf{k})\cdot\mathbf{r}}d\tau. \tag{3.20}$$

Therefore

$$\mathcal{H}_{\mathbf{G}',\mathbf{G}} = \frac{\hbar^2}{2m_0\Omega}\int |\mathbf{G}+\mathbf{k}|^2 e^{i(\mathbf{G}-\mathbf{G}')\cdot\mathbf{r}}d\tau + \frac{1}{\Omega}\int e^{-i(\mathbf{G}'+\mathbf{k})\cdot\mathbf{r}}V_c e^{i(\mathbf{G}+\mathbf{k})\cdot\mathbf{r}}d\tau. \tag{3.21}$$

The first integral (over all space) of Eq. (3.20) has a value only if
G' = G, in which case it is equal to the normalization volume Ω introduced before. By making use of the Kronecker delta, Eq. (3.21) can be written as,

$$\mathcal{H}_{\mathbf{G},\mathbf{G}'} = \frac{\hbar^2}{2m_0}|\mathbf{G}+\mathbf{k}|^2\delta_{\mathbf{G},\mathbf{G}'} + V \tag{3.22}$$

where V is the potential given by,

$$V = \frac{1}{\Omega}\int e^{-i(\mathbf{G}'+\mathbf{k})\cdot\mathbf{r}}V_c e^{i(\mathbf{G}+\mathbf{k})\cdot\mathbf{r}}d\tau. \tag{3.23}$$

Remembering that the aim of this work is to be able to calculate microscopic properties of a crystal the potential V is defined such that is depended on some yet undefined potential V_c located at every atomic site $\mathbf{r}_a$ given by

$$V_c = \sum_{\mathbf{r}_a} V_a(\mathbf{r}-\mathbf{r_a}). \tag{3.24}$$

From Eq.(3.24) and Eq. (3.23) V can be written as

$$V = \frac{1}{\Omega}\int e^{-i(\mathbf{G}'+\mathbf{k})\cdot\mathbf{r}}\sum_{\mathbf{r_a}} V_a(\mathbf{r}-\mathbf{r}_a)e^{i(\mathbf{G}+\mathbf{k})\cdot\mathbf{r}}d\tau \tag{3.25}$$

Therefore

$$V = \frac{1}{\Omega}\sum_{\mathbf{r_a}}\int V_a(\mathbf{r}-\mathbf{r}_a)e^{-i(\mathbf{G}-\mathbf{G}')\cdot\mathbf{r}}d\tau. \tag{3.26}$$

As the origin for the summation over the atoms is undefined, then it is possible, and mathematically convenient to perform the transformation $\mathbf{r}\rightarrow\mathbf{r}+\mathbf{r}_a$, then we obtain [54].

$$V = \frac{1}{\Omega}\sum_{\mathbf{r}}\int V_a(\mathbf{r}_a)e^{i(\mathbf{G}-\mathbf{G}')\cdot(\mathbf{r}+\mathbf{r_a})}d\tau. \tag{3.27}$$

and therefore

$$V = \frac{1}{\Omega} \sum_{\mathbf{r_a}} e^{i(\mathbf{G}-\mathbf{G}')\cdot\mathbf{r_a}} \int V_a(\mathbf{r}_a) e^{i(\mathbf{G}-\mathbf{G}')\cdot\mathbf{r}} d\tau. \tag{3.28}$$

Where the term $\sum_{\mathbf{r}_a} e^{i(\mathbf{G}-\mathbf{G}')\cdot\mathbf{r}_a}$ is known as the geometric structure factor S. Since the atomic sites within the crystal are constructed from the Bravais lattice plus the basis, then the sum over the atomic sites can be replaced with two separate summations, i.e one over the Bravais lattice points and the other one over the points in each basis such that [54],

$$S = \sum_{\mathbf{R}} \sum_{\mathbf{t}} e^{i(\mathbf{G}-\mathbf{G}')\cdot(\mathbf{R}+\mathbf{t})} \tag{3.29}$$

where $\mathbf{R}$ is a Bravais lattice vector and $\mathbf{t}$ is a basis vector. Hence

$$S = \sum_{\mathbf{R}} e^{i(\mathbf{G}-\mathbf{G}')\cdot\mathbf{R}} \sum_{\mathbf{t}} e^{i(\mathbf{G}-\mathbf{G}')\cdot\mathbf{t}} \tag{3.30}$$

The scalar product of a Bravais lattice vector with a reciprocal lattice vector is just an integral number of 2π [54], i.e.

$$\mathbf{G}'' \cdot \mathbf{R} = 2\pi n, n \in Z. \tag{3.31}$$

Therefore, $e^{i(\mathbf{G}-\mathbf{G}')\cdot\mathbf{R}} = 1$, and hence for N Bravais lattice points in the crystal we have [54],

$$S = N \sum_{\mathbf{t}} e^{i(\mathbf{G}-\mathbf{G}')\cdot\mathbf{t}}. \tag{3.32}$$

In a case of a compound structure e.g GaAs with an atom basis having a face centered Bravais lattice the atoms are positioned in a manner such that $\mathbf{t} = \pm\mathbf{T}$, where,

$$\mathbf{T} = \frac{A_0}{8}(\hat{i} + \hat{j} + \hat{k}). \tag{3.33}$$

Because the nature of the material is such that it contains two different types of atoms i.e. Ga and As, the summation for the structure factor in Eq. (3.29) becomes:

$$S = N[e^{i(\mathbf{G}-\mathbf{G}')\cdot\mathbf{T}} + e^{-i(\mathbf{G}-\mathbf{G}')\cdot\mathbf{T}}]. \tag{3.34}$$

Then from Eq. (3.34) it is easy to notice that

$$\begin{aligned} S = N[&\cos(\mathbf{G}-\mathbf{G}')\cdot\mathbf{T} + i\sin(\mathbf{G}-\mathbf{G}')\cdot\mathbf{T} \\ &+ \cos(\mathbf{G}-\mathbf{G}')\cdot\mathbf{T} - i\sin(\mathbf{G}-\mathbf{G}')\cdot\mathbf{T}] \end{aligned} \tag{3.35}$$

and therefore

$$S = 2N\cos(\mathbf{G}-\mathbf{G}')\cdot\mathbf{T}. \tag{3.36}$$

The geometric structure factor potential in Eq. (3.25) can be re-written using Eq. (3.34) as

$$V = \frac{2N}{\Omega}\cos(\mathbf{G}-\mathbf{G}')\cdot\mathbf{T}\int V_a(\mathbf{r})e^{i(\mathbf{G}-\mathbf{G}'\cdot\mathbf{r})}d\tau \tag{3.37}$$

For face centered crystal structure the primitive cube of side A_0 (lattice constant) contains four Bravais lattice (i.e eight atoms), and hence,

$$\Omega_c = \frac{A_0^3}{4}. \tag{3.38}$$

Also re-witting $\mathbf{G}'-\mathbf{G}$ as the vector $\mathbf{q}$, then

$$V = \frac{2}{\Omega_c}\cos(\mathbf{q}\cdot\mathbf{T})\int V_a(\mathbf{r})e^{-i\mathbf{q}\cdot\mathbf{r}}d\tau \tag{3.39}$$

and now from Eq. (3.39) the factor

$$\frac{1}{\Omega_c}\int V_a(\mathbf{r})e^{-i\mathbf{q}\cdot\mathbf{r}}d\tau = V_f(q) \tag{3.40}$$

is the Fourier transform of the undefined atomic potential V_a and can be labelled conveniently as $V_f(q)$ where $q = |\mathbf{q}|$ and this term is known as the atomic form factor potential [14]. The form factor represent many microscopic properties of a crystal. For diamond structure crystal such as Si, the atomic form factor potential $V(q)$ would include the $1s^2 2s^2 2p^6$ electrons [54]. The remaining four valence electrons, which in an isolated, Si atom are found in the $3s$ and $3p$ orbital, are the subject of the investigation and it is their energy levels and charge distribution which determine the electronic properties of the crystal [54]. The atomic form factor potential $V(q)$ is a discrete function, only having non-zero values for a particular value of q [54]. $V(q)$ has only three non-zero values, which occurs for $q = \sqrt{3}$,$\sqrt{8}$ and $\sqrt{11}$. In the case of a compound semiconductor with two different atoms (with the cation at $-\mathbf{T}$), and the anion at $\mathbf{T}$, where $\mathbf{T}$ is given in Eq. (3.33) we see that,

$$V = \frac{N}{\Omega}\sum_{\mathbf{t}} e^{i(\mathbf{G}-\mathbf{G}')\cdot\mathbf{t}}\int V_a(\mathbf{r})e^{i(\mathbf{G}-\mathbf{G}')\cdot\mathbf{r}}d\tau \tag{3.41}$$

where N is just the number of different atoms. Summing over the two basis positions i.e.

$-\mathbf{T}$ and at $\mathbf{T}$ we have

$$\begin{aligned} V =& \frac{N}{\Omega} e^{-i(\mathbf{G}-\mathbf{G}')\cdot\mathbf{T}} \int V_a^{cat}(\mathbf{r}) e^{i(\mathbf{G}-\mathbf{G}')\cdot\mathbf{r}} d\tau \\ &+ \frac{N}{\Omega} e^{-i(\mathbf{G}-\mathbf{G}')\cdot\mathbf{T}} \int V_a^{an}(\mathbf{r}) e^{i(\mathbf{G}-\mathbf{G}')\cdot\mathbf{r}} d\tau \qquad . \end{aligned} \tag{3.42}$$

Remembering that $N/\Omega = 1/\Omega_c$, and also that the fact that $\mathbf{q} = \mathbf{G}' - \mathbf{G}$, then we obtain,

$$V = e^{-i(\mathbf{G}-\mathbf{G}')\cdot\mathbf{T}} \frac{1}{\Omega_c} \int V_a^{cat}(\mathbf{r}) e^{-i(\mathbf{q}\cdot\mathbf{r})} d\tau + e^{i(\mathbf{G}-\mathbf{G}')\cdot\mathbf{T}} \frac{1}{\Omega_c} \int V_a^{an}(\mathbf{r}) e^{-i(\mathbf{q}\cdot\mathbf{r})} d\tau \tag{3.43}$$

From Eq. (3.40) the pseudopotential form factor for the anion and the cation can be seen as,

$$V_f(q) = \frac{1}{\Omega_c} \int V_a^{an}(\mathbf{r}) e^{-i(\mathbf{q}\cdot\mathbf{r})} d\tau \tag{3.44}$$

and

$$V_f(q) = \frac{1}{\Omega_c} \int V_a^{cat}(\mathbf{r}) e^{-i(\mathbf{q}\cdot\mathbf{r})} d\tau \tag{3.45}$$

respectively and therefore it follows that

$$V = V_f^{cat}(q) e^{-(\mathbf{G}-\mathbf{G}')\cdot\mathbf{T}} + V_f^{an}(q) e^{(\mathbf{G}-\mathbf{G}')\cdot\mathbf{T}} \tag{3.46}$$

Equation (3.44) can be manipulated easily by making use of trigonometric facts such as,

$$\sin x = \frac{e^{ix} - e^{-}ix}{2i}$$

$$\cos x = \frac{e^{ix} + e^{-}ix}{2}$$

to give

$$\begin{aligned} V =& [V_f^{an}(q) + V_f^{cat}(q)] \cos(\mathbf{G} - \mathbf{G}'\cdot)T \\ &+ [V_f^{an}(q) - V_f^{cat}(q)] \sin(\mathbf{G} - \mathbf{G}'\cdot)T. \end{aligned} \tag{3.47}$$

Often the sum i.e. $[V_f^{an}(q) + V_f^{cat}(q)]$ and the difference i.e.$[V_f^{an}(q) - V_f^{cat}(q)]$ of the pseudopotential form factors is labeled symmetric and anti-symmetric form factors .i.e. V_f^S and V_f^A respectively. Then Eq. (3.44) can be written as

$$V = V_f^S(q) \cos(\mathbf{G} - \mathbf{G}'\cdot)\mathbf{T} + iV_f^A(q) \sin(\mathbf{G} - \mathbf{G}'\cdot)\mathbf{T} \tag{3.48}$$

Substituting Eq. (3.48) into Eq. (3.23) we get the Hamiltonian matrix for all the elements of the matrix given by,

$$\begin{aligned} \mathcal{H}_{\mathbf{G},\mathbf{G}'} =& \frac{\hbar^2}{2m_0} |\mathbf{G} + \mathbf{k}|^2 \delta_{\mathbf{G},\mathbf{G}'} + V_f^S(q) \cos(\mathbf{G} - \mathbf{G}') \cdot \mathbf{T} \\ &+ iV_f^A(f) \sin(\mathbf{G} - \mathbf{G}')\cdot\mathbf{T} \end{aligned} \tag{3.49}$$

The atomic form factor potential $V_f(q)$ are parameter that can be obtained by fitting to experimental data. For the superlattices calculations the emperical pseudopotential form factor are represented by a continuous curve. For our calculations we develop a continuous form factor potential by making use of Levenberg-Marquardt algorithm together with the cubic spline interpolation. This will be explained in details in the chapter Four.

3.4 Extension of the empirical pseudopotential method to layered structures: the Large basis approach

In this chapter the extension of the pseudopotential method to large basis approximation is explained. The generalization of the EPM is needed in the case of calculating the electronic structure of layered structures such as superlattices quantum wells,quantum wires and quantum dots. From the expression for the crystal potential which is given by,

$$V = \frac{1}{\Omega}\sum_{\mathbf{r}_a} e^{i(\mathbf{G}-\mathbf{G}')\cdot\mathbf{r}_a}\int V_a(\mathbf{r})e^{i(\mathbf{G}-\mathbf{G}')\cdot\mathbf{r}}d\tau \tag{3.50}$$

Once again expressing $\mathbf{q} = \mathbf{G} - \mathbf{G}'$ we get,

$$V = \frac{\Omega_c}{\Omega}\sum_{r_a} e^{-i\mathbf{q}\cdot\mathbf{r_a}}\frac{1}{\Omega_c}\int V_a(\mathbf{r})e^{-q\cdot\mathbf{r}}d\tau \tag{3.51}$$

where Ω_c is the volume of the primitive cell. The normalized integral of the atomic potential $V_a(\mathbf{r})$ is still the pseudopotential form factor, although now it is acknowledged that the generalization may allow for many atom types at, as yet, unspecified positions and so it is important to write [54]:

$$\frac{1}{\Omega_c}\int V_a(\mathbf{r})e^{-i\mathbf{q}\cdot\mathbf{r}}d\tau \qquad \text{as} \qquad V_f^{\mathbf{r}_a}(q) \tag{3.52}$$

therefore the emperical pseudopotential form factor of the atom at position $\mathbf{r}_a$ is:

$$V = \frac{\Omega_c}{\Omega}\sum_{r_a} e^{-i\mathbf{q}\cdot\mathbf{r_a}}V_f^{\mathbf{r}_a}(q). \tag{3.53}$$

where q in $V_f^{\mathbf{r}_a}(q)$ is the magnitude of the difference of the lattice vectors i.e. $q = ||G-G||$. Just as in the case of the bulk semiconductor, the atomic positions can be written as a

sum of the Bravais lattice vector and a basis vector such that,

$$\mathbf{r}_a = \mathbf{R} + \mathbf{t} \tag{3.54}$$

and thus it follows from Eq. (3.54) and Eq. (3.53) that,

$$V = \frac{\Omega_c}{\Omega} \sum_{\mathbf{R}} e^{-i\mathbf{q}\cdot\mathbf{R}} \sum_{\mathbf{t}} e^{-i\mathbf{q}\cdot\mathbf{t}} V_f^{\mathbf{r}_a}(q) \tag{3.55}$$

Once again the scalar product of the reciprocal lattice vector, $\mathbf{q} = \mathbf{G} - \mathbf{G}'$, with Bravais lattice vector, $\mathbf{R}$, will be equal to the integral multiple of 2π, and hence $e^{i\mathbf{q}\cdot\mathbf{R}} = 1$ and if there are N of these new generalized bases in the total volume of the crystal, then we have,

$$V = \frac{\Omega_c N}{\Omega} \sum_{\mathbf{t}} e^{-i\mathbf{q}\cdot\mathbf{t}} V_f^{\mathbf{r}_a}(q) \tag{3.56}$$

If we let Ω_b to be the total volume of the crystal Ω divided by the number of the new general Bravais lattice points N, the volume occupied by its primitive cell would be:

$$V = \frac{\Omega_c}{\Omega_b} \sum_{\mathbf{t}} e^{-i\mathbf{q}\cdot\mathbf{t}} V_f^{\mathbf{r}_a}(q) \tag{3.57}$$

In the case of the diamond or zinc blende crystal structure with two atom basis the volume of the primitive cell Ω_c is the volume occupied by two atoms. In general the basis with N_a atoms the volume occupied by its primitive cell would be,

$$\Omega_b = \frac{N_a}{2}\Omega_c \tag{3.58}$$

and therefore the expression for the crystal potential will be,

$$V = \frac{2}{N_a} \sum_{\mathbf{t}} e^{-i\mathbf{q}\cdot\mathbf{t}} V_f^{\mathbf{r}_a}(q) \tag{3.59}$$

so that the equation for the Hamiltonian matrix elements is

$$\mathcal{H}_{\mathbf{G},\mathbf{G}'} = \frac{\hbar^2}{2m_0}|\mathbf{G} + \mathbf{k}|^2 \delta_{\mathbf{G},\mathbf{G}'} + \frac{2}{N_a} \sum_{\mathbf{t}} e^{-i\mathbf{q}\cdot\mathbf{t}} V_f^{\mathbf{r}_a}(q) \tag{3.60}$$

Equation (3.60) is the generalized equation for the Hamiltonian matrix elements. By making certain choices of the basis and the primitive cell, Eq. (3.60) can be used to calculate the electronic structure of heterostructures of all dimensions, i.e. quantum wells, wires, and dots [54].

3.5 Inclusion of spin-orbit coupling

In band theory, the spin orbit interactions are responsible for the splitting of the degenerate energies. For most semiconductor materials the splitting occur on the valence bands near the zone center i.e. $\Gamma = 0$. In developing the spin-dependent solution the basis set must contain spin-dependent (s or s') terms, and therefore the matrix elements of the Hamiltonian given in Eq. (3.18) which is expressed as,

$$\mathcal{H}_{\mathbf{G}',\mathbf{G}} = \int u^*_{\mathbf{G}',\mathbf{k}} \mathcal{H} u_{\mathbf{G},\mathbf{k}} d\tau \tag{3.61}$$

can be written out as

$$\mathcal{H}_{\mathbf{G}',s',(\mathbf{G},s)} = \int u^*_{\mathbf{G}',\mathbf{k},s'} \mathcal{H} u_{\mathbf{G},\mathbf{k},s} d\tau \tag{3.62}$$

In the large basis approach the spin-orbit coupling potential V_{SO} is the sum over the contributions from all the N_a atoms within the basis, and in the analogy of the crystal potential Eq. (3.59) is,

$$V_{SO} = \frac{1}{N_a} \sum_t e^{i\mathbf{q}\cdot\mathbf{t}} [-i\lambda^{\mathbf{r}_a} (\mathbf{G}' + \mathbf{k}) \times (\mathbf{G} + \mathbf{k}\cdot) \sigma_{s',s}] \tag{3.63}$$

where once again $\mathbf{q} = \mathbf{G}' - \mathbf{G}$. and $\lambda^{\mathbf{r}}_a$ is a parameter quantifying the magnitude of the interaction [54]. the superscript $\mathbf{r}_a$ indicates that λ is depended upon the atomic species at all the basis sites within the unit cell [54]. The entity $\sigma_{s',s} = \langle s'|\sigma|s\rangle$ where:

$$\sigma = \sigma_1 \hat{\mathbf{i}} + \sigma_2 \hat{\mathbf{j}} + \sigma_3 \hat{\mathbf{k}} \tag{3.64}$$

where σ_1, σ_2 and σ_3 are the Pauli spin matrices which are given by,

$$\sigma_1 = \begin{pmatrix} 0 & 1 \\ 1 & 0 \end{pmatrix} \sigma_2 = \begin{pmatrix} 0 & -i \\ i & 0 \end{pmatrix} \sigma_3 = \begin{pmatrix} 1 & 0 \\ 0 & -1 \end{pmatrix} \tag{3.65}$$

and thus,

$$\sigma = \begin{pmatrix} \hat{\mathbf{k}} & \hat{\mathbf{i}} - i\hat{\mathbf{j}} \\ \hat{\mathbf{i}} + i\hat{\mathbf{j}} & -\hat{\mathbf{k}} \end{pmatrix} \tag{3.66}$$

3.6 Inclusion of other effects

The spin orbit couplings are not the only effects which can be taken into account when calculating the electronic structure of semiconductor materials. The many body effects and non-local effects can also be included for electronic structure calculations. To date there is no literature that suggest that the many body effects can be included successfully in the frame work of the emperical pseudopotential method, However, these effects can be included in the multiband $\mathbf{k} \cdot \mathbf{p}$ [72], and the density functional theory [38, 60].

The local pseudopotential approximation has provided sufficient explanation to the optical data available for semiconductor compounds, however, there are some discrepancies in the results of the local pseudopotential approximation when compared to experiment [17]. The results of the local pseudopotential calculations when compared to the valence bands of high-resolution photoemission results, i.e., x-ray photoemission spectroscopy [73, 74], ultraviolet photo emission spectroscopy [75, 76] reveal that the local EPM calculations obtain incorrect valence bands width, in the majority of cases [17]. Band topologies and optical critical point symmetries calculated by a local pseudopotential for Ge and GaAs have been found to be in error [77]. In addition to this other one-electron approaches (which correspond to energy dependent nonlocal pseudopotentials) produced more accurate results for the valence bands than the local EPM approach [74].

These discrepancies led to suspicions that a purely local pseudopotential technique could not produce satisfactory results, thus a refined nonlocal pseudopotential calculations should be performed to supplement and extend on the earlier local EPM calculations [17]. In Refs. [15, 17, 78, 79, 80, 81] the inclusion of the nonlocal effects in the pseudopotential method is described. Chelikowsky and Cohen [79] calculated the bandstructure of GaAs by employing a nonlocal pseudopotential, in their calculation they also included the spin-orbit coupling, excellent agreement with electroreflectance was achieved. Kim [15] investigated the electronic bandstructure of various crystal orientations of relaxed and strained bulk, 1D and 2D confined semiconductors using nonlocal empirical pseudopotential method with spin-orbit interaction. Brust [80] examined the electronic structure of three group-IV elements using a nonlocal pseudopotential.

Several effects can be included within the frame work of the emperical pseudopotential method. The inclusion of other effects is mainly to produce results which can be comparable to experiments. In this work we only consider the inclusion of the spin-orbit coupling in our calculations.

Chapter 4

Levenberg-Marquardt Optimization Applied to Cubic Spline Interpolation

4.1 Introduction

In this Chapter we introduce the Levenberg-Marquardt (least squares) optimization technique and show how it may be applied to fit a piece wise cubic spline interpolation to an arbitrary function. In particular we will demonstrate the accession made at the start of this thesis about more rapid convergence properties of the cubic spline interpolation compared to a linear combination of Gaussian functions. We begin with a brief description of the Levenberg-Marquardt algorithm (LMA).

4.2 Levenberg-Marquardt optimization

The Levenberg-Marquardt algorithm is the most widely used technique applicable in solving the nonlinear least- square problems. The LMA is mostly used to provide a

solution to the problem of non-linear least squares by way of minimization. The least square problem come about when fitting function to a set of data point by minimizing the the sum of the squares of the errors between the data points and the function [82]. The LMA is actually a combination of two minimization methods i.e. the gradient-decent method and the Gauss-Newton method. The LMA acts more like the gradient decent method when the parameters are far from their optimal value, and acts more like the Gauss-Newton method when the parameters are closer to their optimal value [82].

Over the years LMA has become a standard tool for solving nonlinear optimization problems in a wide variety of fields. The popularity of the method stems from the fact that it significantly outperforms gradient descent and conjugate gradient methods in the optimization of medium sized nonlinear models [83]. Consider the problem of fitting a function $\tilde{y} = g(\tilde{x}, \boldsymbol{\alpha})$ to a set of m given data points (x_k, y_k), $k = 1, 2, \ldots, m$. Here $\tilde{x}$ is an independent variable and $\boldsymbol{\alpha} = (\alpha_1, \alpha_2, \ldots \alpha_n)$ is a vector of the system parameters, with $n < m$. To solve this problem it is convenient to minimize the sum of the weighted squares of the errors (or weighted residuals) between the measured data and the fitted function, i.e. to minimize the quantity [82]

$$\begin{aligned} \chi^2(\boldsymbol{\alpha}) &= \frac{1}{2}\sum_{k=1}^{m}\left(\frac{y(x_k) - \tilde{y}(x_k, \boldsymbol{\alpha})}{w_k}\right)^2 \\ &= \frac{1}{2}\mathbf{y}^T\mathbf{W}\mathbf{y} - \mathbf{y}^T\mathbf{W}\tilde{\mathbf{y}} + \frac{1}{2}\tilde{\mathbf{y}}^T\mathbf{W}\tilde{\mathbf{y}}. \end{aligned} \tag{4.1}$$

In Eq. (4.1) the $m \times m$ weighting matrix $\mathbf{W}$ is diagonal, with $W_{kk} = 1/w_k^2$. Traditionally there are two methods to obtain the minimum: the gradient descent (or steepest descent) and Gauss-Newton methods [84]. According to the gradient descent method the perturbation $\mathbf{h}_{gd}$ that moves the parameters in the direction of steepest descent towards the minimum is given by

$$\mathbf{h}_{gd} = \beta\mathbf{J}^T\mathbf{W}(\mathbf{y} - \tilde{\mathbf{y}}), \tag{4.2}$$

where $\mathbf{J}$ is the Jacobian matrix of the function g, and β is a positive scalar that determines the the length of the step. According to the Gauss-Newton method the required perturbation is given by $\mathbf{h}_{gn}$, where

$$\left[\mathbf{J}^T\mathbf{W}\mathbf{J}\right]\mathbf{h}_{gn} = \mathbf{J}^T\mathbf{W}(\mathbf{y} - \tilde{\mathbf{y}}). \tag{4.3}$$

The LMA adaptively varies the parameter updates between the gradient descent and Gauss-Newton update, i.e.

$$\left[\mathbf{J}^T\mathbf{W}\mathbf{J} + \lambda\mathbf{1}\right]\mathbf{h}_{lm} = \mathbf{J}^T\mathbf{W}\left(\mathbf{y} - \tilde{\mathbf{y}}\right), \tag{4.4}$$

where small values of the algorithmic parameter λ result in a Gauss-Newton update and large values of λ result in a gradient descent update. At a large distance from the function minimum, the gradient descent method is utilized to provide steady and convergent progress towards the solution. As the solution approaches the minimum, λ is adaptively decreased and the LMA approaches the Gauss-Newton method, for which the solution typically converges more rapidly to the local minimum. The update relationship suggested by Marquardt [85] is given by

$$\left[\mathbf{J}^T\mathbf{W}\mathbf{J} + \lambda\mathrm{diag}\left(\mathbf{J}^T\mathbf{W}\mathbf{J}\right)\right]\mathbf{h}_{lm} = \mathbf{J}^T\mathbf{W}\left(\mathbf{y} - \tilde{\mathbf{y}}\right). \tag{4.5}$$

In this work we make use of the Python function `leastsq()`, which provides an efficient implementation of the LMA, to minimize the residual $\mathbf{y} - \tilde{\mathbf{y}}$, i.e. the difference between the target and the fitting function. For simplicity, in the following sections, we will denote the residual simply as $\mathbf{R} \equiv \mathbf{y} - \tilde{\mathbf{y}}$

4.3 Cubic spline interpolation

For a more efficient approximation, a piecewise polynomial approximation with higher odder pieces is needed [86]. Any smooth function that is piecewise polynomial, and is also smooth where the polynomial connects can be regarded as a spline [87]. A piecewise polynomial function $f(x)$ is obtained by dividing x into contiguous intervals, and representing $f(x)$ by separate polynomial in each interval. At the endpoints i.e. knots the polynomials are joined together such that a degree of smoothness of the resulting function is achieved. If a functions $f(x)$ is twice continuously differentiable, i.e. $f(x)$ has a first and a second derivative then $f(x)$ is a cubic spline. The cubic spline approximating function continues to be the most popular choice for interpolating and approximation [86].

We subdivide the interval $[0, q_{max}]$ into n equidistant sub-intervals, each having a length a. The function $f(q)$ is the expanded in terms of the cubic spline as follows. For q contained within the i-th subinterval $[q_i, q_{i+1}]$, where $i = 0, 1, \ldots, n-1$,, the cubic spline interpolation of $f(q)$ is given by

$$f(q) = C_{1,i} + q\left(C_{2,i} + \frac{q}{2}\left(C_{3,i} + \frac{q}{3}\right)\right), \tag{4.6}$$

where $a = q_{max}/n = q_{i+1} - q_i$. Continuity of $f(q)$ and $f'(q)$ between the ith and the $(i+1)$th subinterval then requires,

$$\frac{1}{6}C_{4,i}a^3 + \frac{1}{2}C_{3,i}a^2 + C_{2,i}a + C_{1,i} = C_{1,i+1} \tag{4.7}$$

and

$$\frac{1}{2}C_{4,i}a^2 + C_{3,i}a + C_{2,i} = C_{2,i+1}\ . \tag{4.8}$$

Solving for $C_{3,i}$ and $C_{4,i}$ in Eq. (4.7) and Eq. (4.8) gives

$$C_{3,i} = -\frac{1}{a^2}(-6C_{1,i+1} + 6C_{1,i} + 4aC_{2,i} + 2C_{2,i+1}a) \tag{4.9}$$

$$C_{4,i} = \frac{1}{a^3}(-12C_{1,i+1} + 12C_{1,i} + 6aC_{2,i} + 6C2, i+1a) \tag{4.10}$$

now substituting Eq. (4.10) and Eq. (4.9) into Eq. (4.6) we get

$$\begin{aligned} f(q) &= \frac{1}{a^3}(a-q)^2(a+2q)C_{1,i} + \frac{1}{a^2}(a-q)^2qC_{2,i} \\ &+ \frac{1}{a^3}q^2(3a-2q)C_{1,i+1} + \frac{1}{a^2}q^2(q-a)C_{2,i+1} \end{aligned} \tag{4.11}$$

where $C_{1,i}, C_{2,i}, C_{1,i+1}$ and $C_{2,i+1}$ are our cubic spline coefficients, $a = q_{max}/n$, q_{max} is the maximum interval and n is the number of the intervals. The polynomials appearing in Eq. (4.11) are the orthogonal Hermite polynomials:

$$\begin{aligned} h_0(s) &= (1-s)^2(1+2s) \\ h_1(s) &= (1-s)^2 s \\ h_2(s) &= s^2(3-2s) \\ h_3(s) &= s^2(s-1) \end{aligned}$$

such that,

$$\begin{aligned} h_0'(s) &= 6s(s-1) \\ h_1'(s) &= (3s-1)(s-1) \\ h_2'(s) &= -6s(s-1) \\ h_3'(s) &= s(3s-2) \end{aligned}$$

4.4 Application of the LMA to cubic spline interpolation of CAFFPs

The knowledge of the form factors at a few discrete values of q is normally good enough for accurate bandstructure calculation in bulk material. The discrete values of q are the magnitudes of the differences between the reciprocal lattice vectors i.e. $q = ||\mathbf{G} - \mathbf{G}'||$, of the, usually cubic, reciprocal lattice. In the large basis approach q can have many more value than only a few discrete points. Therefore, the atomic form factor potentials become continuous function of q in the case of layered structures [54]. The large basis approach is also capable of treating bulk material as a special case. In the case of bulk materials the only value of the continuous atomic form factor potentials that enter into the calculations are those at the discrete set of q points mentioned earlier.

Unfortunately there exist no universal atomic form factors. This is due to the differences that exist between the pseudopotential form factor potentials of the same species in different materials [54]. For example, in the case of AlAs/GaAs layered structure the As in AlAs is different to As in GaAs. This is due to the difference that exist in the core potential, i.e. nucleus plus the inner electron shell, of the As atom is different in both materials. This difference is significant for bandstructure calculations, so careful consideration has to be made for layered structure calculations [54].

The idea of using a linear combination of four Gaussians, multiplied by a smoothing function to determine the atomic form factor potentials, $V(q)$, was originally proposed by Mader and Zunger [3]. This idea was mainly proposed in order to circumvents the limitations of other theoretical models such as the effective mass approximation (EMA) and the Kroning-Penney model, to calculate properties of large semiconducting systems with non trivial geometries which includes structurally inhomogeneous quantum structures, such as partially ordered alloys, clustering in alloys, rough interfaces, quantum dots and wires, and nano-meter quantum well [3]. All of these systems require for their description a computational unit cell containing ≈ 1000 atoms [3].

The "folded spectrum method" proposed in Ref. [11] can be used to calculate the electronic structure of systems that require a large supercell with complex geometries. Although such an approach overcomes the limitations of the tight binding model and the effective mass approximation, it is still not good enough for nanostructures. This is because the long wave components of $V(q)$ required for nanostructure, need to be explicitly fitted to properties with larger repeated unit cells, not to bulk zinc blende properties. In addition to this, fitting the binary compounds, AC and BC, does not by itself produce a common C atom needed in the calculation for, AC/BC interfaces. Mäder and Zunger [3] made use of a large number of additional lattice vectors which could be obtained by interpolation [14, 88] or by fitting an algebraic form of the potential to a zinc blende form factor [89].

The crystal potential $V(r)$, can be written as superposition of atomic potentials $v_\alpha(\mathbf{r})$, which is assumed to be spherically symmetric, i.e.

$$\begin{aligned} V(\mathbf{r}) &= \sum_{n,\alpha} v_\alpha(|r - \tau_\alpha - \mathbf{R}_n|) \\ &= \frac{1}{\Omega_c} \sum_{\alpha} \sum_{\mathbf{G}} e^{i\mathbf{G}(\tau_\alpha - r)} v_\alpha(|\mathbf{G}|) \end{aligned} \tag{4.12}$$

where $\sum_{n,\alpha}$, runs over all positions τ_α within the cell as well as the unit cell vectors $\mathbf{R}_n$. $\sum_{\mathbf{G}} e^{i\mathbf{G}}$ runs over all atomic types α, and the reciprocal lattice vector $\mathbf{G}$, Ω_c is the unit cell volume [3]. Choosing the origin in the zinc blende unit cell halfway between the two atoms $\alpha = A$ and $\alpha = C$, Eq. (4.13), can be expressed as,

$$V(\mathbf{r}) = \frac{1}{\Omega_c} \sum_{\mathbf{G}} [\cos(\mathbf{G} \cdot \tau) v_s(G) + i \sin(\mathbf{G} \cdot \tau) v_a] exp(-i\mathbf{G} \cdot \mathbf{r}) \tag{4.13}$$

where $\tau = \frac{a}{8}(111)$ is the atomic positions. $v_s(G) = v_A(G) + v_C(G)$, and $v_a(G) = v_A(G) - v_C(G)$ are the symmetric and antisymmetric respectively, a is the lattice constant [3]. The symmetric and antisymmetric form factor can be adjusted at a small number of zinc blende reciprocal lattice vectors **G** to fit band energies and effective masses at different unit cell volumes Ω_c. **G** vector length scales as $\Omega_c^{-\frac{1}{3}}$ this gives information about the form factors in the neighborhood of each **G** vector [3]. $v_s(G)$ and $v_a(G)$ determined at a range of volumes provided a means of fitting the hydrostatic deformation potentials , i.e. the volumes of the derivatives of the band gaps [3]. By inspecting the obtained ≈ 20 discrete form factors, it was found that v_s and v_a could each be fitted very well by a linear combination of two Gaussians [3]. The atomic potentials $v_A = \frac{1}{2}(v_s + v_a)$ and $v_C = \frac{1}{2}(v_s - v_a)$ can be reconstructed from the form factors [3]. Each atomic pseudopotential $v_\alpha(q)$, is a linear combination of four Gaussians multiplied by a smoothing function:

$$v_\alpha(q) = \Omega_\alpha \sum_{i=1}^{4} a_{i\alpha} e^{-c_{i\alpha}(q-b_{i\alpha})^2}[1 + f_{0\alpha} e^{-\beta_\alpha q^2}] \ , \tag{4.14}$$

where Ω_α, is the atomic normalization volume, $v_\alpha(q)$ is the atomic pseudopotential form factor [3]. The parameters of Eq. (4.14) can be adjusted independently to obtain an optimal fit of $v_\alpha(q)$, may change [3]. For a complete explanation of 4.14 one can see Ref.[3] The (continuous atomic form factor potentials) CAFFPs given by Eq. (4.14) has proved to produce many experimentally observed results for bulk material and such as the band gaps and effective masses [3].

As mentioned in chapter one, a major drawback of using the linear combination of Gaussian functions to interpolate the atomic form factor potentials, is that such functions have poor convergence properties compared to piecewise interpolations. This essential difference occurs because the adjustable coefficients in the linear combination are all interdependent, i.e. when the Levernberg-Marquardt algorithm (or any other optimization algorithm, for that matter) tries to adjust one coefficient it affects the functional form of the whole linear combination. By contrast coefficients of the piecewise interpolation can be optimized independently for each piece of the interpolation.

In Fig 4.1 we illustrate the difference in the convergence rates by using piecewise cubic splines and a linear combination of Gaussians to interpolate a sine function. In this

case a linear combination of four Gaussian functions was used and compared to a cubic spline interpolation over six intervals. Both interpolations require twelve initially unknown

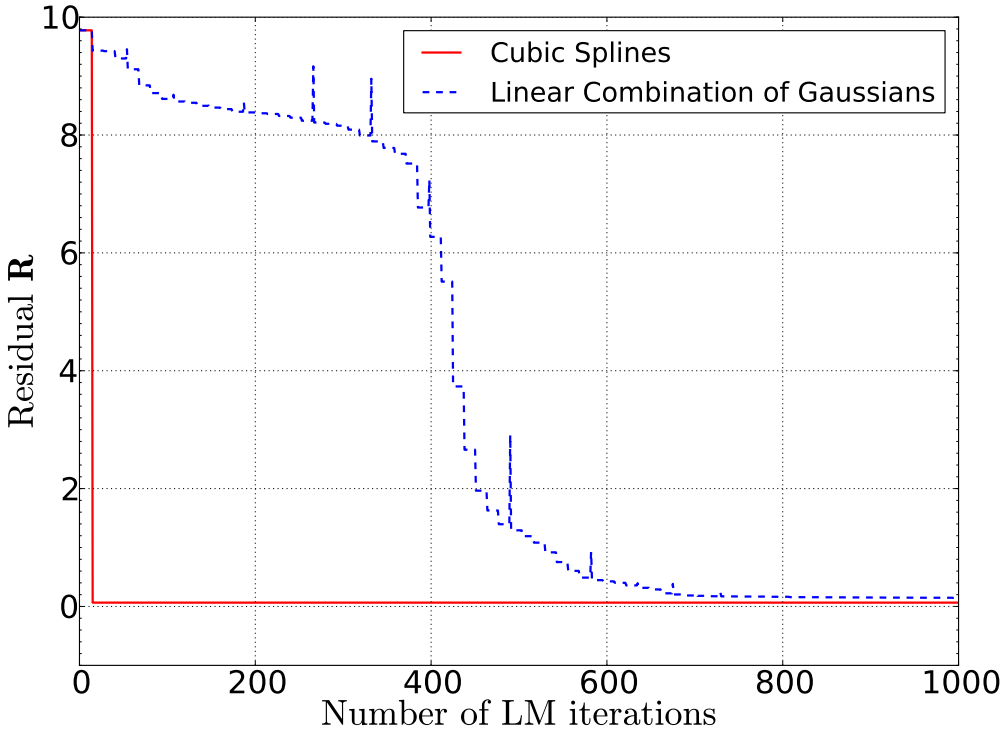

Figure 4.1: Comparison of convergence rate for optimizing the continuous atomic form factors using piecewise cubic spline (solid line) as oppose to linear combination of Gaussians (dash lines) In this case the target function was $\sin(x)$ with $x \in [0, 5]$. The residual $\mathbf{R}$ is the difference between the interpolated and target functions using 500 sample points corresponding to a grid of equally spaced points in the x-domain.

coefficients to be optimized. As can be seen in Fig. 4.1, for the cubic spline interpolation, convergence is achieved within few than 30 iterations, while for the linear combination of Gaussians it takes more than a 1000 iterations to reduce the residual to approximately the same value.

The difference in the rates of convergence shown in Fig. 4.1 are fairly typical independently of the target function used. In trying to optimize the coefficients of the CAFFPs, forming a residual between a target bandstructure and a calculated bandstructure, the difference

between the rates of convergence becomes crucial because the bandstructure calculation which has to be performed for each iteration is computationally expensive.

The cubic spline continuous atomic form factor potentials are determined in the following way: Firstly cubic spline function is interpolated over the discrete points required in the case of bandstructure calculations of bulk semiconductor materials. Our cubic spline function is defined over 25 subintervals. We then use our cubic spline CAFFPs to calculate the bandstructures for GaAs and AlAs as explained in details in chapter six. Excellent results for energy bands are obtained for GaAs and AlAs bandstructures calculated with the interpolated cubic spline continuous form factor potentials.

In order to determine the much needed continuous atomic form factor potentials for layered structure calculations, the Levernberg-Marquardt method, in conjunction with the cubic spline functions are used. In this work we calculate our continuous atomic form factors by optimizing the cubic spline coefficients `C(i,j)`, by fitting to calculated zinc blende bandstructures. The `C(i,j)` are actually responsible for connecting the piecewise polynomials which define the cubic spline functions. The results of the optimized cubic spline CAFFPs for layered structure calculations are presented in chapter six. In the next chapter we provide the Fortran codes and the Python scripts developed for the purpose of this work.

Chapter 5

Method For Numerical Calculations

5.1 Determining the cubic spline continuous atomic form factor potentials

The purpose of this Chapter is to describe the Python scripts and the Fortran codes, developed in this work. Two Fortran subroutines were written in this work for different purposes. One code is written to setup the cubic spline function (see C1) and the other code is written to set up the Hamiltonian matrix to be solved (see C2). These subroutines are wrapped into Python modules using F2PY [90]. Since Fortran is strictly suitable for numeric and scientific computing and Python is an object oriented programming language. To optimize the computational time the numerically intensive parts of this work, like the loading of the matrix elements are done in Fortran.

Python is a scripting language which supports multiple paradigms, including object oriented, imperative and functional programming. Such features including the large and comprehensive standard library, compromises the computational speed, thus the numerically intensive parts of the code are better done in Fortran than in Python. Many important and very useful Python libraries makes it easy to implement some of the important functions of the codes.

Our cubic spline continuous atomic form factor potentials are determined by employing the Levernberg-Marquardt algorithm together with cubic spline interpolations. In order to determine our cubic spline continuous form factor potentials, two important codes were written, one in Fortran and the other one in Python. The function of the Fortran code is to create a subroutine called `smooth` which is wrapped into a Python module using F2PY [90]. `smooth` is a cubic spline interpolation function of form:

$$\begin{aligned} f(q) &= \frac{1}{a^3}(a-q)^2(a+2q)C_{1,i} + \frac{1}{a^2}(a-q)^2 q C_{2,i} \\ &+ \frac{1}{a^3}q^2(3a-2q)C_{1,i+1} + \frac{1}{a^2}q^2(q-a)C_{2,i+1} \end{aligned} \tag{5.1}$$

Here i refers to the ith interval, each interval being of length a. In the Python code we optimize our cubic spline coefficients $C_{i,j}$, which are stored in the array `CC(i,j)`. Starting from arbitrary cubic spline coefficients, our cubic spline continuous atomic form factors are determine as follows. The zinc blende bandstructures calculated from other methods, e.g., DFT, $\mathbf{k}\cdot\mathbf{p}$ and the EPM are used as target bandstructures. The `CC(i,j)`, get optimized by adjusting themselves, such that the residual error between the target bands and the cubic spline calculated bandstructure is reduced to a minimal value. The optimized `C(i,j)`, are written to file so that every time `smooth` is called anywhere in the code, it takes into account the optimized cubic spline coefficients. This procedure is explained in the coming sections, when we describe the Fortran and the Python codes used.

5.2 Codes developed for determining the CAFFPs and for calculating band structures

5.2.1 C1

The subroutine `smooth` is written in Fortran. The purpose of `smooth` is to return cubic spline interpolation `ff` corresponding to coefficients `CC(i,j)`. The coefficients `CC(i,j)` are passed in a vector `v`. `q` is a vector containing the magnitude of the reciprocal lattice

vector at which the form factors are required. `aa` is the interval for piecewise interpolation and `cut` is the cutoff for the interpolated potential. For `q` > `cut` the potential is truncated to zero. `M` is the number of intervals of length `aa` used in the cubic spline interpolation. Using F2PY [90] this code is wrapped into a Python module which can be imported to various Python scripts.

```
subroutine smooth(ff,q,v,aa,cut,N,M)
IMPLICIT REAL*8(A-H,O-Y)
IMPLICIT INTEGER(I-N)
DIMENSION ff(0:N-1),q(0:N-1),v(0:2*M+1)
DIMENSION CC(2,0:M+3)
!f2py intent(in) q, v, aa, cut
!f2py intent(out) ff
! cut is max cut off for q values
! aa is the interval width for cubic spline interpolation
k = 0
N = size(q)
M = (size(v)-2)/2
do j = 0,M+2,2
  CC(1,j)= v(k)
  CC(1,j+1)= v(k+2)
  CC(2,j)= v(k+1)
  CC(2,j+1)= v(k+3)
  k = k + 4
end do
aa = cut/float(M)
do i = 0,N-1
   if (q(i) .GT. cut) then
      ff(i) = 0.0d0
   else
   j = int(q(i)/aa)
```

```
   qd = q(i)-j*aa
   ff(i) = (1.0/(aa**3))*(aa-qd)**2*(aa+2.0*qd)*CC(1,j)&
           +(1.0/(aa*aa))*(aa-qd)**2*qd*CC(2,j) &
           +(1.0/(aa**3))*qd*qd*(3.0*aa-2.0*qd)*CC(1,j+1) &
           +(1.0/(aa**2))*(qd**2)*(qd-aa)*CC(2,j+1) &
   end if
end do
end subroutine
```

5.2.2 C2

This code is written in Fortran. The purpose of this code is to create the Hamiltonian matrix named ZMH. The Hamiltonian matrix created here is generalized to large basis. For two atoms, this code can be used to determine the Hamiltonian Matrix for a compound semiconductor. In the case of large basis, the lattice vectors is increased along the $z-$direction in a spiral. The spin-orbit coupling is taken into account by adding the constant spin-orbit parameters which are passed in as `AFF`. `cj` are the continuous atomic form factor potentials. For zincblende bandstructure calculations say for example GaAs, `cj` will contain the continuous atomic form factor potential for the Ga atom and a continuous atomic form factor potential for the As atom. `GK` is the number of k-points and `GRR` is the lattice vectors. This code is also wrapped into Python module called `slpseudomatrix` using F2PY [90] and can be called with in different Python codes.

```
SUBROUTINE slpseudomatrix(ZMH,A0,GK,GRR,cj,AXY,SOC,MM,M)
IMPLICIT INTEGER (I-N)
IMPLICIT REAL*8 (A-H,O-Y)
IMPLICIT COMPLEX*16 (Z)
PARAMETER (EV = 27.2113961d0, BR = 0.0529177249d0, API = 3.141592654d0)
DIMENSION GRR(0:M-1,0:2), cj(0:1,0:M-1,0:M-1), ZMH(0:M-1,0:M-1)
DIMENSION GK(0:2), GS(0:2),GP(0:2),AXY(0:1,0:3),AFF(0:1)
```

```
!
!f2py intent(in) A0, GK, GRR, cj, AXY, AFF
!f2py intent(out) ZMH
!f2py depend(M) ZMH, GRR, cj
!f2py depend(MM) AFF
!
L = M/2
!open(20,file = 'zmh.dat')

DO J = 0,L-1
   DO I = 0,L-1
      IF (I.NE.J) THEN
         GS = GRR(J,:) - GRR(I,:)
         qs = sqrt(GS(0)**2 + GS(1)**2 + GS(2)**2)
         AB = qs*(2.0d0*API/A0)
         DO K = 0,MM-1
            ZMH(I,J) = ZMH(I,J)+(2.0/REAL(MM))*cj(int(AXY(K,3)),I,J) &
                       *CDEXP(-DCMPLX(0.0D0,DOT_PRODUCT(GS,(AXY(K,0:2)/ &
                       (10.0*BR))))*2.0d0*API/A0)
          ZMH(I+L,J+L) = ZMH(I,J)
          write(20,*) L
         END DO
      END IF
   END DO
END DO

DO I = 0 ,L-1
   GS = GK + GRR(I,:)
   ZMH(I,I) = 0.5d0*DOT_PRODUCT(GS,GS)*(2.0*API/A0)**2
   ZMH(I+L,I+L) = ZMH(I,I)
END DO
```

```
! Add spin-orbit contrbution to Block 1, i.e.(+1/2,+1/2)
DO J = 0,L-1
   DO I = 0,L-1
      IF (I.NE. J) THEN
         GS = GRR(I,:) - GRR(J,:)
         CALL VCP(GK + GRR(I,:), GK + GRR(J,:),GP)
         DO K = 0,MM-1
            ZMH(I,J) = ZMH(I,J)+(1.0/REAL(MM))&
            *CDEXP(-DCMPLX(0.0D0,DOT_PRODUCT(GS,(AXY(K,0:2)/(10.0*BR))))&
            *2.0d0*API/A0)*DCMPLX(-AFF(INT(AXY(K,3))),0.0D0)&
            *DCMPLX(0.0D0,GP(2))*((2.0d0*API)/A0)**2
         END DO
      END IF
   END DO
END DO

! Add spin-orbit contrbution to Block 2, i.e.(+1/2,-1/2)
DO J = L-1,M-1
   DO I = 0,L-1
      IF (I.NE.J) THEN
         GS = GRR(I,:) - GRR(J,:)
         CALL VCP(GK + GRR(I,:), GK + GRR(J,:),GP)
         DO K = 0,MM-1
            ZMH(I,J) = ZMH(I,J)+(1.0/REAL(MM))&
               *CDEXP(-DCMPLX(0.0D0,DOT_PRODUCT(GS,(AXY(K,0:2)/(10*BR))))&
               *2.0d0*API/A0)*DCMPLX(0.0D0,-AFF(INT(AXY(K,3))))&
               *DCMPLX(GP(0),-GP(1))*((2.0d0*API)/A0)**2
         END DO
      END IF
   END DO
```

```
END DO

! Add spin-orbit contrbution to Block 4, i.e.(-1/2,-1/2)
DO J = L-1,M-1
   DO I = L-1,M-1
      GS = GRR(I,:) - GRR(J,:)
      CALL VCP(GK + GRR(I,:), GK + GRR(J,:),GP)
      DO K = 0,MM-1
         ZMH(I,J) = ZMH(I,J)+ (1.0/REAL(MM))&
         *CDEXP(-DCMPLX(0.0D0,DOT_PRODUCT(GS,(AXY(K,0:2)/(10*BR)))) &
         *2.0*API/A0)*DCMPLX(-AFF(INT(AXY(K,3))),0.0D0)&
         *DCMPLX(0.0D0,-GP(2))*((2.0d0*API)/A0)**2
      END DO
   END DO
END DO
END SUBROUTINE


SUBROUTINE VCP(VA,VB,VC)
IMPLICIT REAL*8 (A-H,O-Y)
IMPLICIT COMPLEX*16 (Z)
IMPLICIT INTEGER (I-N)
DIMENSION VA(0:2), VB(0:2), VC(0:2)
VC(0) = VA(1)*VB(2) - VA(2)*VB(1)
VC(1) = VA(2)*VB(0) - VA(0)*VB(2)
VC(2) = VA(0)*VB(1) - VA(1)*VB(0)
END SUBROUTINE
```

5.2.3 C3

This code is written in Python. The function of this code is to optimize the cubic spline coefficients by making use of least squares. This code optimizes `C(i,j)` by finding and reducing the error between zincblende bandstructures. This code makes use of the two codes already explained in this chapter. From `fillhmat` we import `slpseudomatrix` this is for the Hamiltonian matrix. `smooth` is also needed for the CAFFPs. The input files needed are mostly loaded in as data files. For example `bnd` is the target bandstructure and it is loaded in. `SOC` is the spin-orbit parameters, `axy` is the atoms, `v0` and `v1` are the initial guess of cubic spline coefficients `C(i,j)`. The optimized cubic spline `C(i,j)` are written to file named `opt_cc.dat` and will be used in the next code.

```
from fillhmat import slpseudomatrix
from kagiso import smooth
from pylab import *
from scipy.optimize import leastsq
bnd = loadtxt('hpc_GaAs_no.dat')
SOC = loadtxt('spin_orbit.dat')
axy = loadtxt('atoms.xyz')
MM = len(axy)
fk = loadtxt('k.r')
fg = loadtxt('G.r')
v0 = loadtxt('value1.dat')
v1 = loadtxt('value2.dat')
g = open('opt_cc_1.dat','w')
ccc = concatenate((v0,v1))
ccc = concatenate((ccc,SOC))
print len(ccc)
mv = 25
N = len(fg)
h = fg.reshape(3*N,1)
```

```
GRS = concatenate((h,h))
GRR = GRS.reshape(2*N,3)
M = len(GRR)
GS = zeros(3,'d')
BR = 0.0529177249
EV = 27.2113961
A0 = 0.565/BR
tpa = (2.0*pi/A0)
fs = zeros((2,M,M),'d')
cj = zeros((2,M,M),'d')
k = 0
for xv in range(len(axy)):
   for J in range(M):
      for I in range(M):
     GS[:,] = GRR[J,:] - GRR[I,:]
     k = k+1
     q = sqrt(GS[0]**2 + GS[1]**2 + GS[2]**2)
     AB = q
     fs[xv,I,J] = AB*tpa

fs = fs.reshape(2,M**2,1)
cv =  smooth(fs[0,0:(len(fs[0]))],v0,0.2,5)
cv1 = smooth(fs[0,0:(len(fs[0]))],v1,0.2,5)
cv = cv.reshape(130,130)
cv1 = cv1.reshape(130,130)
cj[0] = (cv/2.0)
cj[1] = (cv1/2.0)

def ef(eng,A0,fk,fs,GRR,axy,MM,M,bnd):
   MM = len(axy)
   cv =  smooth(fs[0,0:(len(fs[0]))],eng[0:2*mv+2],0.2,5)
```

```
   cv1 = smooth(fs[0,0:(len(fs[0]))],eng[2*mv+2:4*mv+4],0.2,5)
   cv = cv.reshape(M,M)
   cv1 = cv1.reshape(M,M)
   cj[0] = (cv/2.0)
   cj[1] = (cv1/2.0)
   i = 0
   GK = fk[i,0:3]
   ZMH = slpseudomatrix(A0,GK,GRR,cj,axy,AFF,MM,M)
   E = (EV*eigvalsh(ZMH,'U').real)
   TE = bnd[i,1:131
   for i in range(1,len(fk[:,0]),1):
      GK = fk[i,0:3]
      ZMH = slpseudomatrix(A0,GK,GRR,cj,axy,AFF,MM,M)
      E1 = (EV*eigvalsh(ZMH,'U').real)
      TE1 = bnd[i,0:len(bnd[0,1:])]
      E = concatenate((E,E1))
      TE = concatenate((TE,TE1))
   er = E-TE
   err = sqrt(dot(er,er))
   print err, E[1308] - E[1307], TE[1308] - TE[1307]
   return er

opt, succ = leastsq(ef,ccc,args = (A0,fk,fs,GRR,axy,MM,M,bnd),maxfev=1000)
print opt

for i in range(len(opt)):
print >> g, (opt[i])
g.close()
```

5.2.4 C4

Finally this code solves the Hamiltonian matrix and calculates the energies $E(k)$ for both the bulk and layered semiconductor structures. Notice in this code there a loaded file named `'opt_cc_1.dat'` and `'opt_cc_2.dat'`. These two files contain the optimized cubic spline `C(i,j)` which are incorporated into smooth to produce optimized continuous atomic form factor potentials. Most of the files used here are similar and have the same function as previously reported in other sections. The calculated energies are written to file named `GaAs_ccff_bands_1.dat`.

```
from fillhmat import slpseudomatrix
from kagiso import smooth
from pylab import *
axy = loadtxt('atoms.xyz')
fk = loadtxt('k.r')
fg = loadtxt('G.r')
ccc = loadtxt('opt_cc_1.dat')
ddd = loadtxt('opt_cc_2.dat')
SOC = loadtxt('spin_orbit.dat')
MM = len(axy)
mv = 25
N = len(fg)
h = fg.reshape(3*N,1)
GRS = concatenate((h,h))
GRR = GRS.reshape(2*N,3)
M = len(GRR)
GS = zeros(3,'d')
BR = 0.0529177249
EV = 27.2113961
A0 = 0.565/BR
tpa = (2.0*pi/A0)
```

```
fs = zeros((4,M,M),'d')
cj = zeros((4,M,M),'d')
k = 0
for xv in range(len(axy)):
   for J in range(M):
       for I in range(M):
     GS[:,] = GRR[J,:] - GRR[I,:]
     k = k+1
     q = sqrt(GS[0]**2 + GS[1]**2 + GS[2]**2)
     AB = q
     fs[xv,I,J] = AB*tpa

fs = fs.reshape(4,M**2,1)

cv0 = smooth(fs[0,0:(len(fs[0]))],ccc[0:52],0.2,5)
cv1 = smooth(fs[0,0:(len(fs[0]))],ccc[52:104],0.2,5)
cv2 = smooth(fs[0,0:(len(fs[0]))],ddd[0:52],0.2,5)
cv3 = smooth(fs[0,0:(len(fs[0]))],ddd[52:104],0.2,5)

cv0 = cv0.reshape(M,M)
cv1 = cv1.reshape(M,M)
cv2 = cv2.reshape(M,M)
cv3 = cv3.reshape(M,M)

cj[0] = (cv0/2.0)
cj[1] = (cv1/2.0)
cj[2] = (cv2/2.0)
cj[3] = (cv3/2.0)

f = open('GaAs_ccff_bands_1.dat','w')
```

```
GK = zeros(3,'d')
ZMH = slpseudomatrix(A0,GK,GRR,cj,axy,AFF,MM,M)
E = (EV*eigvalsh(ZMH,'U').real)
vmax = E[14]
#vmax = E[62] for N= 4
#vmax = E[14] for N= 1
#vmax = E[127]for N= 8
for i in range(len(fk[:,0])):
   GK = fk[i,0:3]
   ZMH = slpseudomatrix(A0,GK,GRR,cj,axy,SOC,MM,M)
   E = (EV*eigvalsh(ZMH,'U').real)
   print i,(E[9]-E[7])
   if i <= 40:
      k = -sqrt(dot(GK,GK))
   else:
      k = +sqrt(dot(GK,GK))
   u0 = list(E-vmax)
   u0.insert(0,k)
   for col in u0:
      f.write('%15.7f' % col)
   f.write('\n')
f.close()
print 'Done'
```

Chapter 6

Results and discussion

6.1 Introduction

In most cases electronic bandstructure calculations are the first step in calculating transport properties of semiconductors. In the emperical pseudopotential method, one of the key parameters that needs to be determined in order for accurate electronic bandstructures to be achieved is the atomic form factor potentials. As mentioned in chapter one, the focus of this work is to develop reliable atomic form factor potentials that can be used for bandstructure calculations in the case of layered semiconductor structures. Since there exist no universal atomic form factors, there is always a need to determine the form factors for specific materials.

In this work we make use of cubic spline CAFFPs to calculate the electronic bandstructures of semiconductor materials. One of the advantages of using cubic spline CAFFPs, is that when optimizing the continuous atomic form factors, convergence can be achieved within a short period of time. This is a major advantage because for large systems which are computationally demanding, rapid convergence rate is required in order to reduce computational time. Figure 6.1, illustrate the convergence rate achieved for optimizing the present cubic spline coefficients.

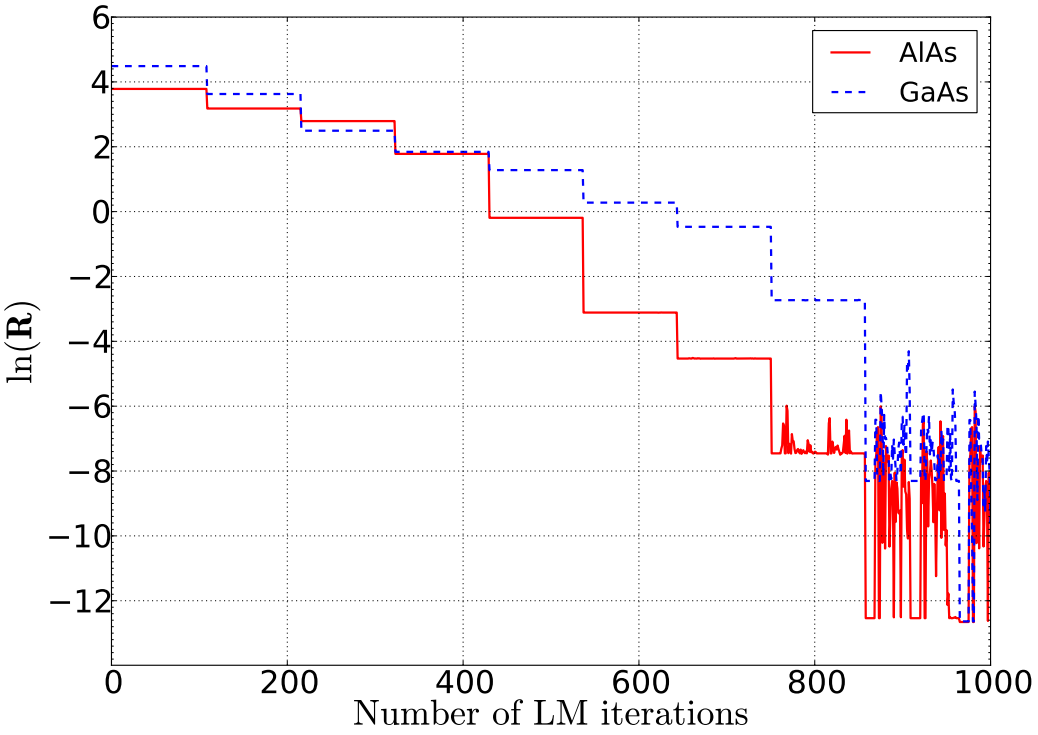

Figure 6.1: Convergence rate for optimizing the continuous atomic form factors potentials used in this work. The residual **R** is the difference between the calculated and target bandstructure. In this case the length of the residual was 1000.

The symmetric and anti-symmetric form factors can be easily determined from the individual atomic form factors by simply making use of $V_f^S = [V_f^{cat}(q) + V_f^{an}(q)]$ and $V_f^A = [V_f^{an}(q) - V_f^{cat}(q)]$. For continuous atomic form factor potentials, the material in which the form factor exist has an effect on the form factor potentials, for example in the case of GaAs and AlAs, the As form factor in GaAs is different to the As in AlAs. Though we don't show in plot the difference between these As continuous form factors potentials, one can be able to see this clearly by comparing the CAFFPs of the As atom in Fig. 6.2 and Fig. 6.6. We mentioned in Chapter one, several different ways in which the form factors can be determined. In chapter four we explained how the atomic form factors were determined in the present work. In the next sections we present the results of using newly determined atomic form factors.

6.2 Bandstructure calculations for GaAs

In this section the cubic spline continuous atomic form factor potentials (CAFFPs), calculated in Chapter five, are used to calculate the electronic bandstructure for GaAs. As mentioned before, for bulk structures like GaAs, the CAFFPs are not necessary, since the bandstructure of such materials can be calculated from the knowledge of the form factors calculated at only a few discrete point of q. However the CAFFPs can also be used for bulk materials. It has been stated in the past Ref. [54], that the CAFFPs can be more suitable for bulk materials since their continuous nature allows for many more point to be taken into account for electronic bandstructure calculations. The atomic form factor potentials in general depends on the type of the material. It makes no difference if the atomic form factors is continuous or discrete, the type of the material has to be taken into consideration. The atomic form factors for GaAs calculated at discrete point of q using the cubic spline CAFFPs are listed in table. 6.1.

Table 6.1: Form factors of GaAs in units of eV calculated at the discrete points of q.

Source	$V_f^S(q)$				$V_f^A(q)$			
	$\sqrt{3}$	$\sqrt{4}$	$\sqrt{8}$	$\sqrt{11}$	$\sqrt{3}$	$\sqrt{4}$	$\sqrt{8}$	$\sqrt{11}$
Ref. [14]	-3.13	-2.33	0.14	0.82	0.95	0.68	0.34	0.14
Ref. [15]	-3.20		0.20	0.94	1.03	0.78		0.83
Ref. [17]	-2.91		0.19	0.92	0.75	0.52		0.01
Present	-3.40	-1.94	0.39	0.72	0.86	0.74	0.26	0.21

The atomic form factors depends on $|\mathbf{q}|$ which is the magnitude of the reciprocal lattice vector. $\mathbf{q}$ itself a reciprocal lattice vector. Since the atomic form factors $V(q)$ is dependent on $|\mathbf{q}|$, $V(q)$ is defined only at the discrete point of q. Figure 6.2 shows the cubic spline CAFFPs and the Gaussian CAFFPs of Ga in GaAs and As in GaAs together with difference between the Gaussian CAFFP and the cubic spline CAFFP. It can seen that both the cubic spline CAFFPs and the Gaussian CAFFPs go through the required discrete values of q. In addition it can be seen that at the points $q = \sqrt{0}, \sqrt{3}, \sqrt{4}, \sqrt{8}$ and $\sqrt{11}$ the difference between the two CAFFPs is essentially zero. A similar fitting procedure is

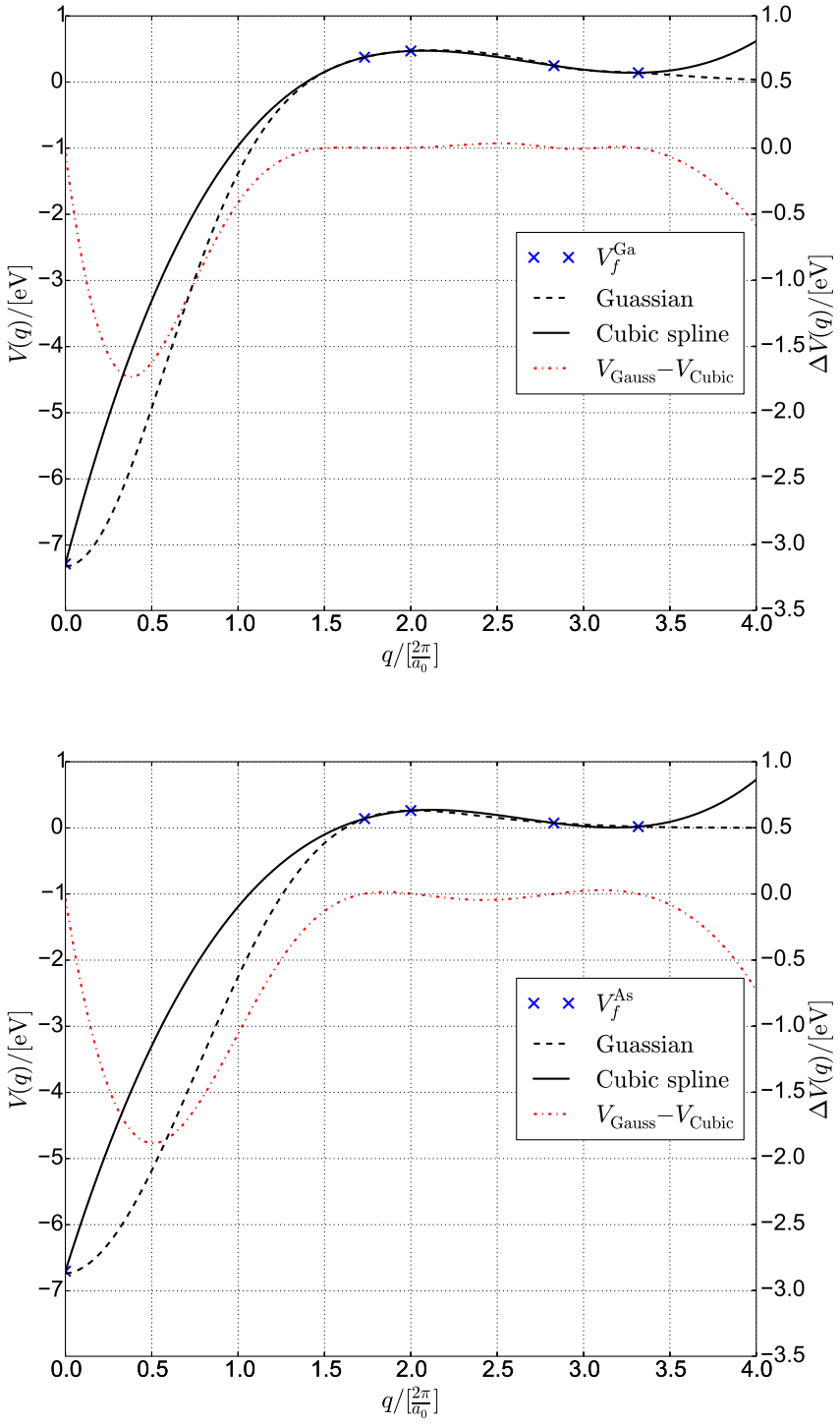

Figure 6.2: Cubic spline CAFFPs and Gaussian CAFFPs of Ga in GaAs (top) and of As in GaAs (bottom) plotted with the differences between the Gaussian CAFFPs and the cubic spline CAFFPs.

performed for As in GaAs, to obtain the complete bandstructure of GaAs, as illustrated in Fig. 6.2.

As in the case of Ga, the CAFFP of As in GaAs also agree well at the discrete points of q, hence one can expect that the resulting bandstructures calculated using both the cubic spline and the Gaussian CAFFPs will have a very close resemblance. In the case of the layered structure calculations it is expected that the difference between the two CAFFPs will somehow affect the bandstructures, this is discussed in detail in section 6.4.

With the CAFFPs of Ga and As the electronic bandstructure of GaAs can be calculated. Listed in table. 6.2 are the energy levels of the bulk GaAs, as obtained from the electronic bandstructure of GaAs calculated in this work. Figures 6.3 and 6.4 illustrates the bandstructures of GaAs calculated using the cubic spline CAFFPs with and without the spin-orbit couplings, respectively, while table. 6.3 summaries the measured energy levels of the bandstructure of GaAs with the inclusion of the spin-orbit couplings. The word relativistic in this work is used in the case of the electronic bandstructure calculated with the inclusion of the spin-orbit coupling.

Good agreement for the energy gap is found between the current results and those obtained through semi-emperical pseudopotential and experiments. Our energy gap is just 0.01 eV below the experimentally obtained energy gap. The word energy gap or band gap E_g in this work is used to refer to the energy difference between the conduction band and the valence band at the zone i.e. at $\Gamma = 0$. The energy gap calculated in this work for GaAs is also in good agreement with the band gap (ΔE_g) reported by Chelikowsky and Cohen [17] in their famous 1976 paper. It should be noted that in their work Chelikowsky and Cohen [17] included the nonlocal effects.

It is expected that the energy gap of the band structure calculated using the cubic spline CAFFPs and the Gaussian CAFFPs will be the same, since it was established in Fig. 6.2, that the difference at the discrete points of q, is essentially very close to zero. However table 6.2 shows that, there is difference of 0.01 eV in calculated band gap. This insignificant difference can be accounted by the difference in the CAFFPs used.

The DFT-LDA results in table 6.2 are just for comparison purpose for detailed explanation of how they were obtained one can see a Ph.D thesis by S. Botti [29]. A close comparison for L_6^v energy level between our results and experiments is found to be 0.01 eV. There is not so much overall difference between our cubic spline CAFFPs bandstructures and the Gaussian CAFFPs bandstructures as can be seen in table 6.2. A difference of 0.01 eV and 0.71 eV is achieved between our results and those obtained experimentally. The overall comparison of our results and the results obtained through experiments is impressive. The only concern is on the Γ_7^c energy level with the calculated difference of 0.71 eV. In order to corrects some of these energy difference and to produce experimentally measured energies, we suggest fitting the atomic form factors to other empirically determined parameters such as effective mass and deformation potentials.

Table 6.2: Comparison of the energy levels (all in electron volt) of bulk GaAs, as obtained in the current work without taking into account the spin-orbit coupling compare to literature.

Energy levels	Present	Gaussians	Experiment	SEMI-EPM[d]	DFT-LDA[d]
Γ_6^v:	-12.17	-12.18	-13.10^a	-12.11	-12.90
ΔE_g	1.51	1.50	1.52^b	1.51	1.37
Γ_7^c:	4.01	4.00	4.72^a	4.01	4.58
X_6^v	-10.03	10.02		-10.00	-10.45
X_6^c	2.05	2.01	1.98^c	2.02	2.12
X_6^c	2.41	2.37	2.38^c	2.39	2.39
L_6^v	-10.68	-10.68		-10.64	-11.19
L_6^c	1.82	1.79	1.81^c	1.83	-1.79
L_6^c	4.86	4.82		4.84	5.46

[a] T. C. Chiang *et al.* [91]

[b] D. D. Sell [92]

[c] D. E. Aspen *et al.* [93]

[d] S. Botti [29]

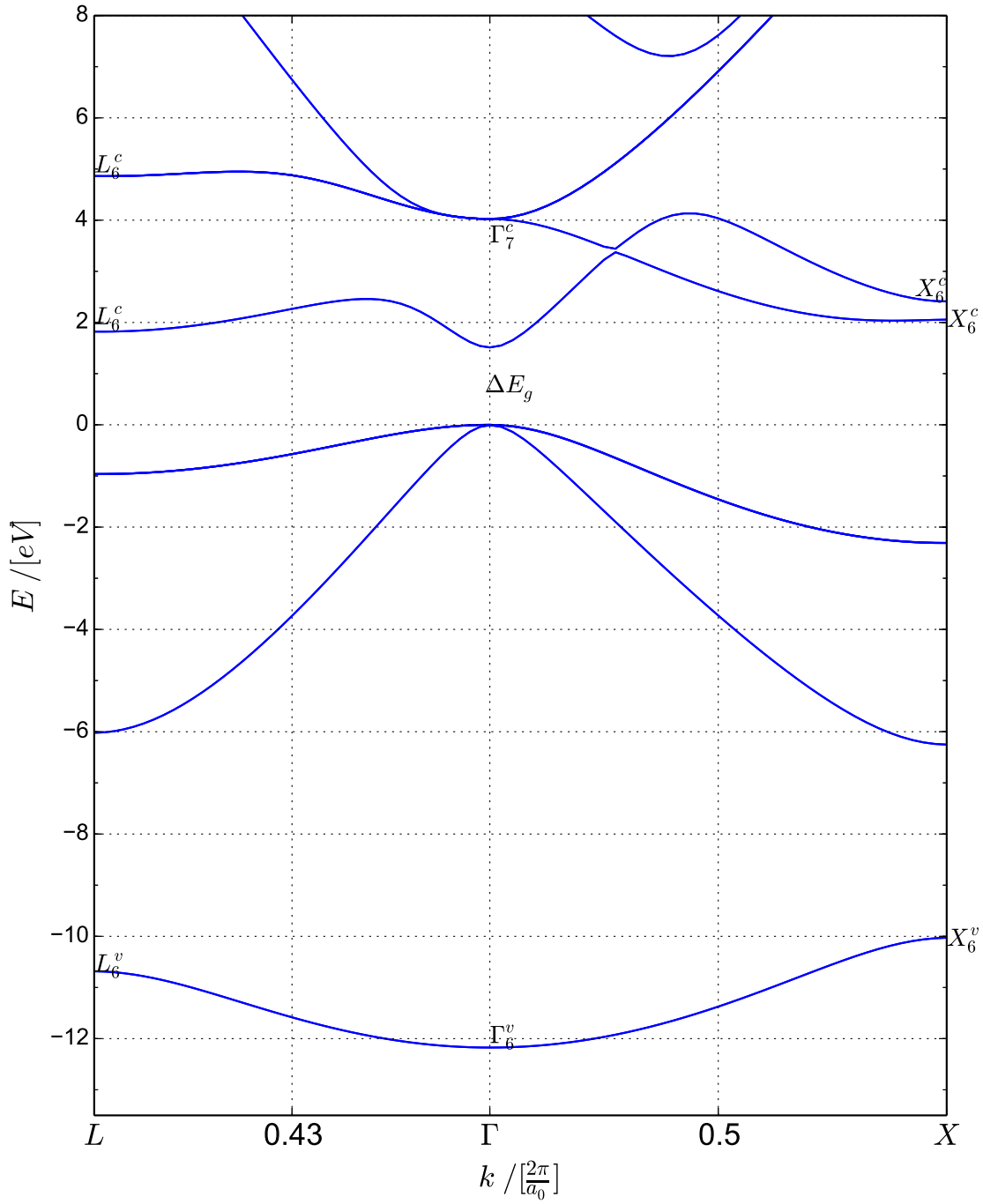

Figure 6.3: Bandstructure of GaAs plotted from $L[\frac{1}{2},\frac{1}{2},\frac{1}{2}]$ to $\Gamma[0,0,0]$ and to $X[0,0.1]$, calculated without the spin-orbit coupling for 65 lattice vectors with a lattice constant of 5.65 Å. The bands have been scaled to have the zero in energy at the maximum of the upper-most valence band.

In other energy level the comparison between the present work and literature is within (0.05 eV and 0.38 eV), this difference can be accounted by the fact that our CAFFPs were determined by optimizing the cubic spline coefficients, by calculating the residual error between the Gaussian and the cubic spline CAFFPs at the discrete points of q, unlike in Ref. [3], where the atomic form factor were fitted to other empirically determined properties like the effective mass and deformation potentials.

The inclusion of the relativistic effects in the bandstructure structure calculations offer more accurate knowledge of the electronic properties of the material [54]. Usually this is done by incorporate the spin-orbit couplings into the bandstructure calculations as explained in Chapter three. Figure 6.4 shows the bandstructure of GaAs calculated with the inclusion of the spin-orbit couplings. Microscopically analyzing Fig. 6.4 shows that near the zone center i.e. $\Gamma = 0$ there are two bands degenerate. The first two bands are called the heavy-hole and the light hole bands. The third band is the spin-orbit split-off band (Δ_{SO}). The split between the heavy-holes and the light-holes is not measured in this work but usually is to close by a few tens to a few hundreds of meV. The effects of spin-orbit couplings in zinc-blende semiconductors is well explained in Refs. [52, 57].

Table 6.3: Comparison of the energies levels (all in electron volt) of GaAs with the inclusion of the spin orbit coupling as obtained in the present work to literature.

Energy levels (eV):	Present	Gaussians	Experiment	Ref. [3]
Γ_6^v:	-12.25	-12.30	-13.10^a	-12.22
ΔE_g	1.44	1.38	1.52^c	1.52
Γ_7^c:	4.86	3.77	4.49^b	4.52
X_6^v	-10.03	-10.14		
X_6^c	2.00	1.90	1.98	2.08
Δ_{SO}	0.24	0.35	0.34^b	0.34

[a] T. C. Chiang *et al.* [91]

[b] D. D. Sell [92]

[c] D. E. Aspen *et al.* [93]

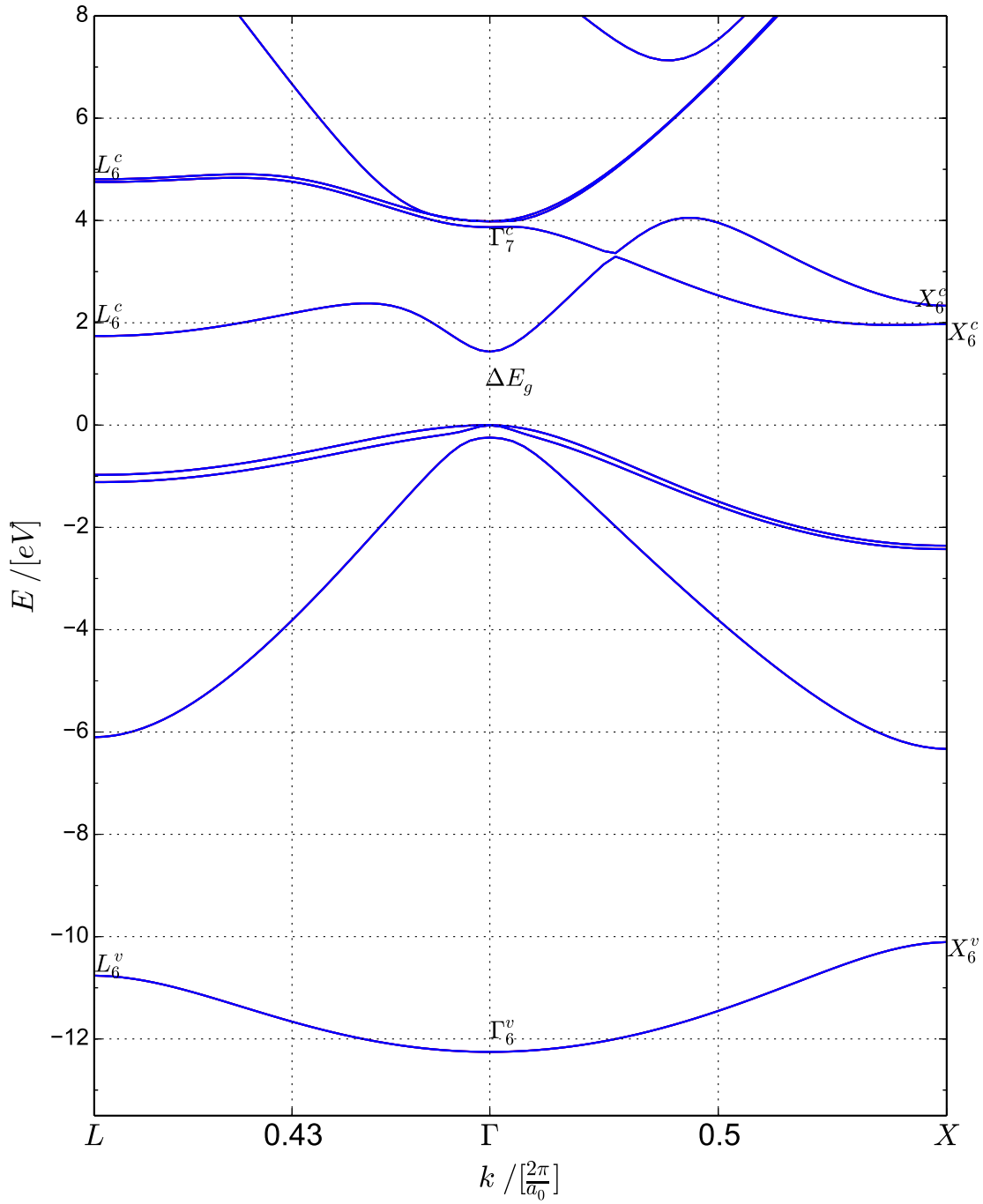

Figure 6.4: Bandstructure of GaAs plotted from $L[\frac{1}{2},\frac{1}{2},\frac{1}{2}]$ to $\Gamma[0,0,0]$ and to $X[0,0,1]$, calculated with the inclusion of the spin-orbit coupling for 65 lattice vectors. with a lattice constant of 5.56 Å. The bands are calculated to have the zero in energy at the maximum of the upper-most valence band.

The spin-orbit split-off Δ_{SO} band calculated in this work by employing the cubic spline CAFFPs has been determined to be 0.24 eV, while that calculated using the Gaussian CAFFPs is 0.34 eV. The difference of 0.1 eV, is due to the fact that the Gaussian CAFFPs, takes into account the spin-orbit coupling effects, while in the case of the cubic spline CAFFPs, the atomic form factors were only fitted to the bandstructures calculated without the spin-orbit coupling and therefore the effects due to spin-orbit couplings were omitted. A difference of 0.08 eV calculated for the band gap of the bandstructures calculated with the Gaussian CAFFPs and the cubic spline CAFFPs, is also due to the different ways in which cubic spline CAFFPs and Gaussian CAFFPs were fitted. The drop in the energy gap from 1.51 eV to 1.44 eV in the case of cubic spline calculated bandstructure, and 1.50 eV to 1.44 eV in the case of Gaussian calculated bandstructure, is attributed by the fact that constant spin-orbit coupling parameters, instead of k-dependent spin-orbit coupling, were used in setting up the Hamiltonian matrix.

Some of the measured energy levels calculated in this work are listed in table 6.3 and comparison is made between this work and literature. In table 6.3 fairly good agreement between the current energy levels and that of Ref. [3] is realized with only a difference of 0.03 eV for Γ_6^c. The present results is also in good agreement with experimental results with a difference of 0.02 eV for X_6^c. The reason why the energy gap decreased from 1.51 eV (non-relativistic) to 1.44 eV (relativistic) is because constant spin-orbit couplings were used instead of the momentum dependent spin-orbit couplings.

6.3 Bandstructure calculations for AlAs

Before the bandstructures of AlAs can be calculated, reliable form factor potentials are needed. Just like in the case GaAs, as discussed in section 6.2, for a complete bandstructure calculations the continuous atomic form factor potential of As in AlAs, and Al in AlAs needs to be determined. We follow a similar procedure as in the case of GaAs reported in section 6.2. The Atomic form factor potentials calculated at the discrete points of q for $AlAs$ are listed in table 6.4. Unfortunately there is not enough literature on

the discrete atomic form factor potentials of AlAs and so we can not list other obtained atomic form factor potentials of AlAs.

Table 6.4: Form factors of AlAs in units of eV calculated at the discrete points of q.

Source	$V_f^S(q)$				$V_f^A(q)$			
	$\sqrt{3}$	$\sqrt{4}$	$\sqrt{8}$	$\sqrt{11}$	$\sqrt{3}$	$\sqrt{4}$	$\sqrt{8}$	$\sqrt{11}$
Present	−3.05	−1.56	0.92	1.2	1.17	1.06	0.83	0.73

Once again the CAFFPs of As in AlAs is different to that of As in GaAs, or any compound structure that has As atoms, and therefore a CAFFP of As in AlAs needs to be determined. Figure 6.5 shows the Gaussian and the cubic spline continuous atomic form factor potentials plotted together with the difference between the two CAFFPs. Figure 6.6

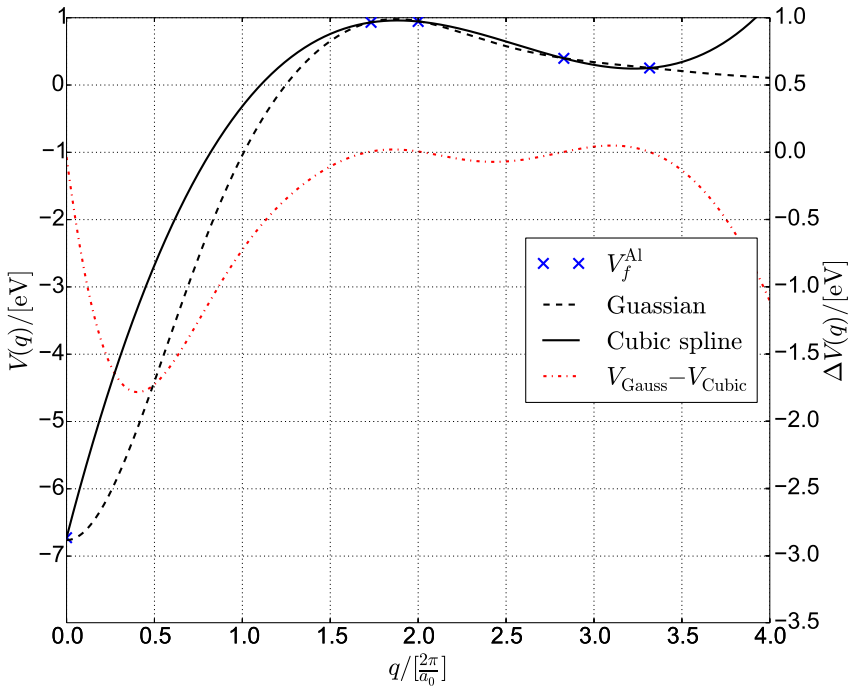

Figure 6.5: Cubic spline CAFFPs and Gaussian CAFFPs of Al in AlAs plotted together with the difference between the Gaussian CAFFPs and the cubic spline CAFFPs.

shows the cubic spline and the Gaussian continuous atomic form factor potentials of As in AlAs, plotted together with the difference between the two continuous form factors. Once again a close examination of Fig. 6.5 and Fig. 6.6 reveal that at the discrete points

the difference between the two form factors is close to zero. With the CAFFPs of the Al

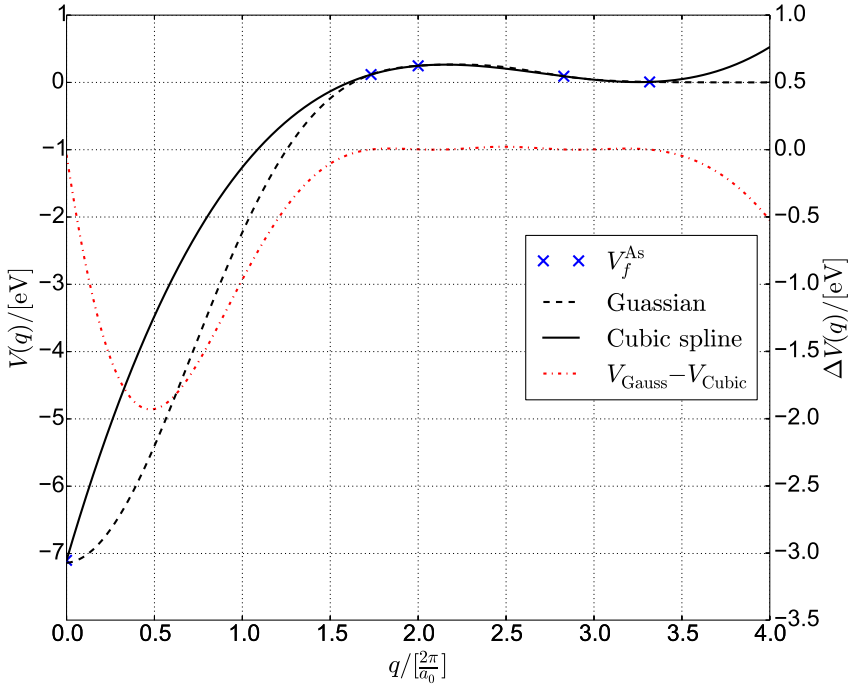

Figure 6.6: Cubic spline CAFFPs and Gaussian CAFFPs of Al in AlAs plotted together with the difference between the Gaussian CAFFPs and the cubic spline CAFFPs.

in AlAs and that of As in AlAs having been determined, calculating the bandstructure for AlAs can follow easily.

Figure. 6.7 displays the bandstructure for AlAs calculated using the cubic spline CAFFPs without the spin orbit couplings. As it can be seen in Fig. 6.7 AlAs has the minimum conduction band at X, and so the energy gap of AlAs can be calculated indirectly between $\Gamma = 0$ and X. But for the purpose of this work, the band gap i.e. ΔE_g is calculated at the zone i.e. $\Gamma = 0$ center directly. The calculated energies of Fig. 6.7 are listed in table 6.5. Examining the contents of table 6.5 shows that there is not so much difference between the energies calculated using the Gaussian and the cubic spline CAFFPs. This is of course expected since both the CAFFPs pass through the required discrete point which are necessary for the bulk bandstructure calculations.

A major difference between the energies obtained through the Gaussian and the cubic

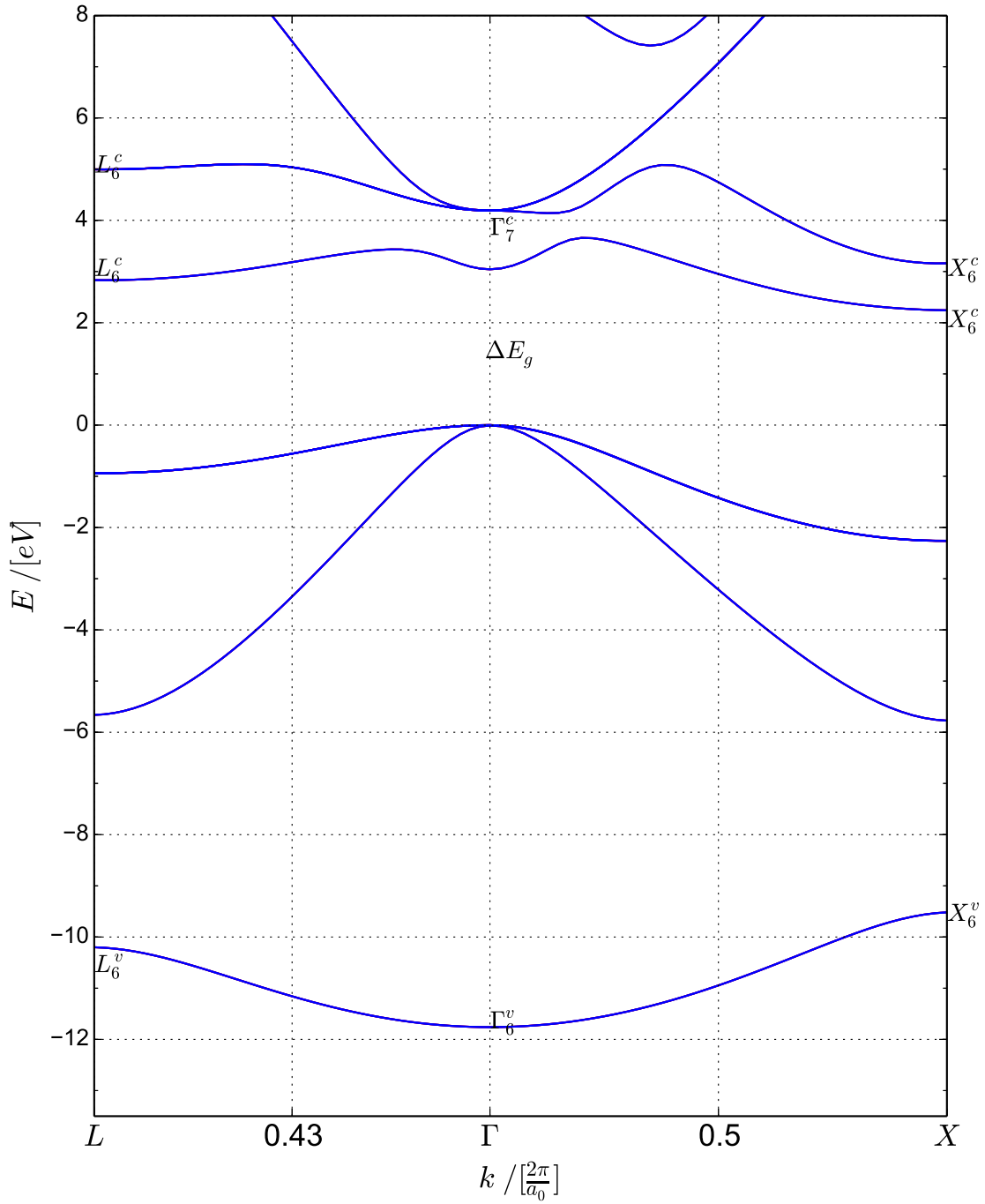

Figure 6.7: Bandstructure of AlAs plotted from $L[\frac{1}{2}, \frac{1}{2}, \frac{1}{2}]$ to $\Gamma[0, 0, 0]$ and then to $X[0, 0, 1]$, calculated without the spin-orbit coupling for 65 lattice vectors with a lattice constant of 5.65 Å. The bands have been scaled to have the zero in energy at the maximum of the upper-most valence band.

spline CAFFPs is at X_6^c where a difference of 0.09 eV i recorded. A difference of 0.05 eV was also recorded for the X_6^v energy level. This is due to similar reason explained in the case of GaAs in section 6.2. The fact that the results obtained in this work produces a band gap i.e. ΔE_g of 3.04 eV which is the same as achieved in Ref. [3] is pleasing, taking into consideration that in Ref. [3], the atomic form factors were fitted to other empirically measured properties such as effective masses and deformation potentials . A difference of 0.07 eV, between the band gap calculated in this work and that obtained through experiments, illustrates the strength of our cubic spline CAFFPs. The relativistic bandstructure for AlAs calculated in this work is displayed in Fig. 6.8. Following on Fig. 6.8 is table 6.6 which list the energies of the bandstructure of AlAs calculated with the inclusion of the spin-orbit couplings. Again the reduction of ΔE_g from 3.04 to 2.97 eV (cubic spline CAFFPs) and from 3.04 eV to 2.91 eV (Gaussian CAFFPs) in both cases is due to the employment of the constant spin-orbit coupling parameters instead of the k-

Table 6.5: Comparison of the energy levels (in electron volt) of bulk AlAs, as obtained in the current work without taking into account the spin-orbit coupling to literature and experiment.

Energy levels:	Present	Gaussians	Experiment	Ref. [3]	Semi-EPM[a]	DFT-LDA[a]
Γ_6^v:	-11.76	-11.76		-11.68	-11.67	-12.03
ΔE_g	3.04	3.04	3.11[c]	3.04	3.03	3.03
Γ_7^c:	4.19	4.18	4.34[d]	4.21	4.21	5.11
X_6^v	-9.65	-9.60			-9.49	-10.01
X_6^c	2.24	2.20	2.23[b]	2.24	2.22	2.21
X_6^c	3.21	3.12			3.20	3.11
L_6^v	-10.20	-10.20			-10.14	-10.57
L_6^c	2.83	2.81	2.54[d]	2.87	2.87	2.99

[a] S. Botti [29]

[b] B. Monemar [94]

[c] D. Wolford [95]

[d] A. Onton [96]

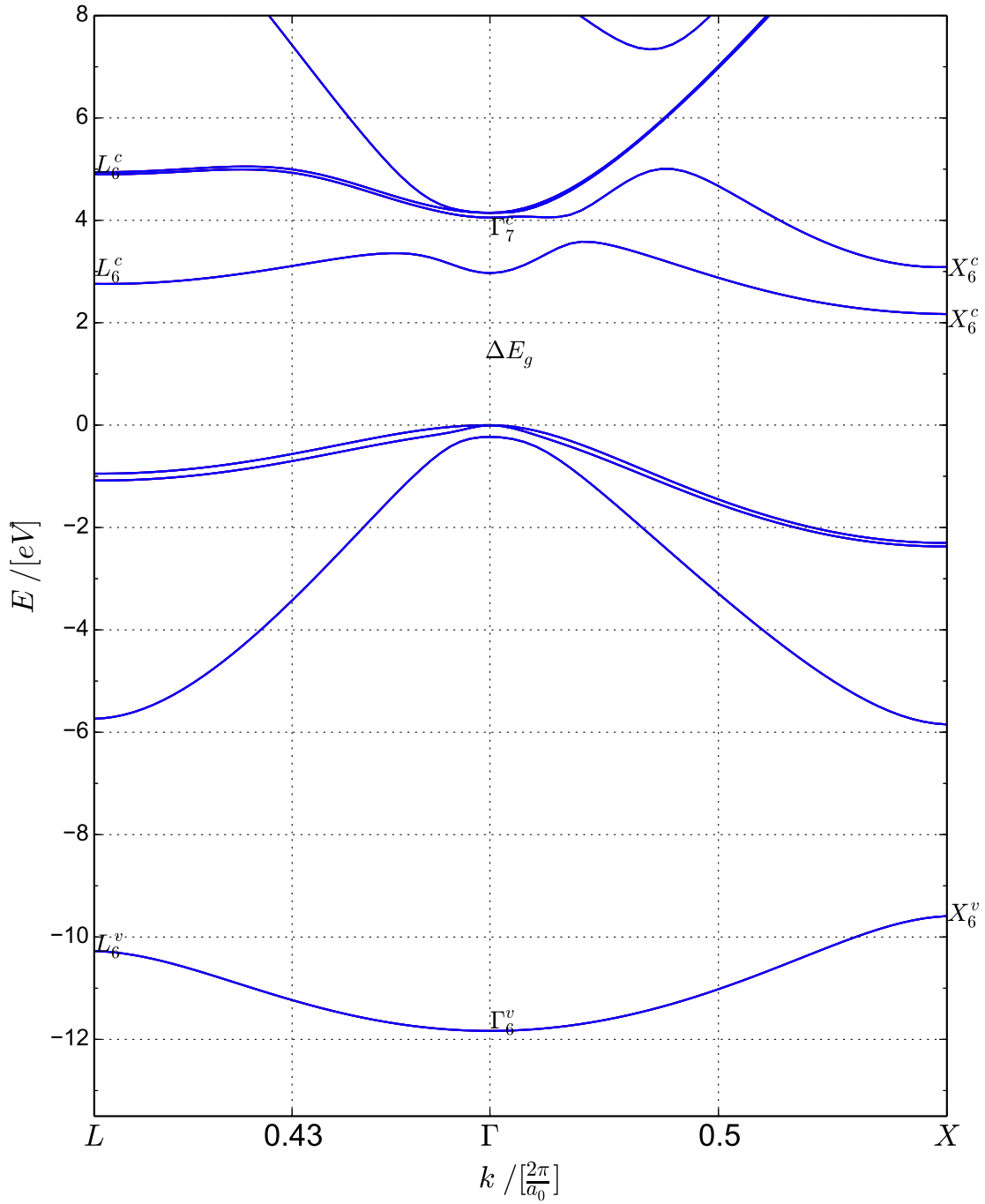

Figure 6.8: Bandstructure of AlAs plotted from $L[\frac{1}{2},\frac{1}{2},\frac{1}{2}]$ to $\Gamma[0,0,0]$ and then to $X[0,0,1]$, calculated with the spin-orbit couplings. The bands have been scaled to have the zero in energy at the maximum of Table 6.6 contains the results of the relativistic bandstructures shown in Fig. 6.8. The band gap measurements for the Gaussian and the cubic spline CAFFP the upper-most valence band.

dependent spin-orbit couplings. For a better agreement in ΔE_g, it is suggested in Ref. [3] that a non-local pseudopotential be incorporated in the calculations. The comparison of other energy levels at the special points Γ, L and X is satisfactory with the difference being in the range of $0.01 - 0.16$ eV, for the energies calculated in this work, experiments and Ref. [3].

Table 6.6: Comparison of the energy level (all in electron volt) of bulk AlAs, as obtained in the current work with spin-orbit coupling to literature.

Energy levels:	Present	Gaussians	Experiment	Ref. [3]
Γ_6^v:	-11.83	-11.87		
ΔE_g	2.97	2.91	3.13[a]	3.05
Γ_7^c	3.23	2.91	4.34[b]	4.36
X_6^c	2.17	2.10	2.23[a]	2.27
L_6^c	5.00	4.86	2.54[c]	2.82
Δ_{SO}	0.22	0.33	0.28[b]	0.31

[a] B. Monemar [94]

[b] A. Onton [96]

[c] D. E. Aspen *et al.* [93]

6.4 AlAs/GaAs superlattice bandstructure calculations

Finally all is in place for the calculation of the $(AlAs)_n/(GaAs)_n$ bandstructures. Since AlAs and GaAs are closely lattice matched [41], the lattice constant of 5.65 Åwill be used for the $(AlAs)_n/(GaAs)_n$ superlattice, and therefore the superlattice are assumed to be strain free. As mentioned before the atomic form factor of As in GaAs is not the same as the atomic form factor of As in AlAs. The difference is due to the difference in the core potential i.e. nucleus plus the inner electron shell, of the As atom is different in both

materials [54]. In addition to this, in a AC/BC superlattice it is expected that the atomic form potential of the C atom will be similar to that in the bulk AC region and that of C inside BC will be similar to that of bulk BC. However at the interface the C atom can have different number of nearest neighbor atoms, so neither the atomic form potential of C in AC nor that C in BC are appropriate.

In this work we follow a similar approach as in Ref. [97]. Here we assume that the interfaces are infinitely thin, so an electron is either in an AC region or in a BC region [3]. This allow for the use of two different C atomic form potentials fitted in AC and BC as reported in section 6.2 and section 6.3. Furthermore, since the is no strain in the layers of our superlattice and a common lattice constant of 5.65 Å is used in this work, there is therefore no difference between AlAs/GaAs and GaAs/AlAs. The period of the superlattice reported here is for $n = 1, 4$ and $n = 8$ with the grown in the z-direction i.e. (001). The reason we avoided calculations beyond $n = 8$, is due to the fact that the matrix size to be solved increases with the number of layers, and therefore this might be demanding computationally as explained in Chapter one.

The superlattice bandstructures will be plotted from R, to Γ and to M this is because our main interest is to calculate band gaps at these special points. Figures 6.9, 6.10 and 6.11 shows the bandstructure $(\mathrm{AlAs})_n/(\mathrm{GaAs})_n$ for $n = 1, 4$ and 8 respectively. Following on these figures is table 6.7 which compares the results of the present work to theory and experiments. Table 6.8 compare the band gap measured at R, Γ and M of $(\mathrm{AlAs})_n/(\mathrm{GaAs})_n$ for $n = 1, 4$ and 8, calculated without the spin orbit coupling.

The spin-orbit interactions are the interaction between the spin-induced magnetic moment and the magnetic field as experienced by an electron [15]. The effects of spin-orbit couplings in band theory are well documented in Refs. [15, 16, 54]. In most cases the spin-orbit interactions are responsible for splitting of the degenerate energies. For most semiconductor material the splitting occur on the valence bands near the zone i.e. $\Gamma = 0$. In Figs. 6.9, 6.10 and 6.11 the splitting of degenerate bands along the wave vector k can be observed. At $\Gamma = 0$, we have the spin split-off band, as the wave k increases the doubly degenerate bands split in to the heavy hole and the light hole. The valence band splitting

is not calculated in this work but in most cases it just a few hundreds of mill-electron volts. Munzar [98] calculated the heavy-hole-light hole splitting in GaAs/AlAs superlattices by employing Eppenga's [99] six band $\mathbf{k}\cdot\mathbf{p}$ for the description of the valence band of GaAs/AlAs superlattices.

The present results compared to experiments show that the band gap obtained in the this work has a difference of 0.22 eV for $n = 1$ and 0.21 eV for $n = 4$. For $n = 4$ the comparison is between the present work and that from Ref. [3] shows a difference of 0.1 eV which is not too bad. Our results reveals that there is no much difference between the energy gap calculated using the cubic spline CAFFPs and the Gaussian CAFFPs for the energy gap. The difference in the energy gaps between the Gaussian CAFFPs and the cubic spline CAFFPs is 0.02 eV for $n = 4$ and 0.11 eV for $n = 8$, for $n = 1$ the measured energy gaps are equal.

Table 6.7: Comparison of the energy gap, ΔE_g (in electron volt) of $(\mathrm{GaAs})_n/(\mathrm{AlAs})_n$ as obtained in the present work with the inclusion of the spin-orbit coupling to experiments and other theoretical models.

Fundamental energy gap ΔE_g				
No. of layers	Present	Gaussians	Experiment [100]	Ref. [3]
1	1.98	1.98	2.20	2.02
4	1.98	1.96	2.19	2.08
8	1.85	1.96		1.91

Table 6.8: Comparison of the energy gaps calculated by the cubic spline CAFFPs and the Gaussian CAFFPs measured at R, Γ and M (in electron volt) of $(\mathrm{GaAs})_n/(\mathrm{AlAs})_n$ without spin orbit coupling.

Number of layers	Cubic spline CAFFPs			Gaussian CAFFPs		
	R	Γ	M	R	Γ	M
1	2.80	1.98	4.34	2.78	1.97	4.33
4	2.82	1.98	2.84	2.77	1.96	2.82
8	2.79	1.98	2.84	2.77	1.96	2.82

The energy difference between the cubic spline and the Gaussian CAFFPs bandstructures at the special point is between 0.01 and 0.05 eV. The contents of table 6.8 suggest that there is not so much significance between the bandstructures of $(GaAs)_n/(AlAs)_n$, obtained by employing the cubic spline CAFFPs and the Gaussian CAFFPs.

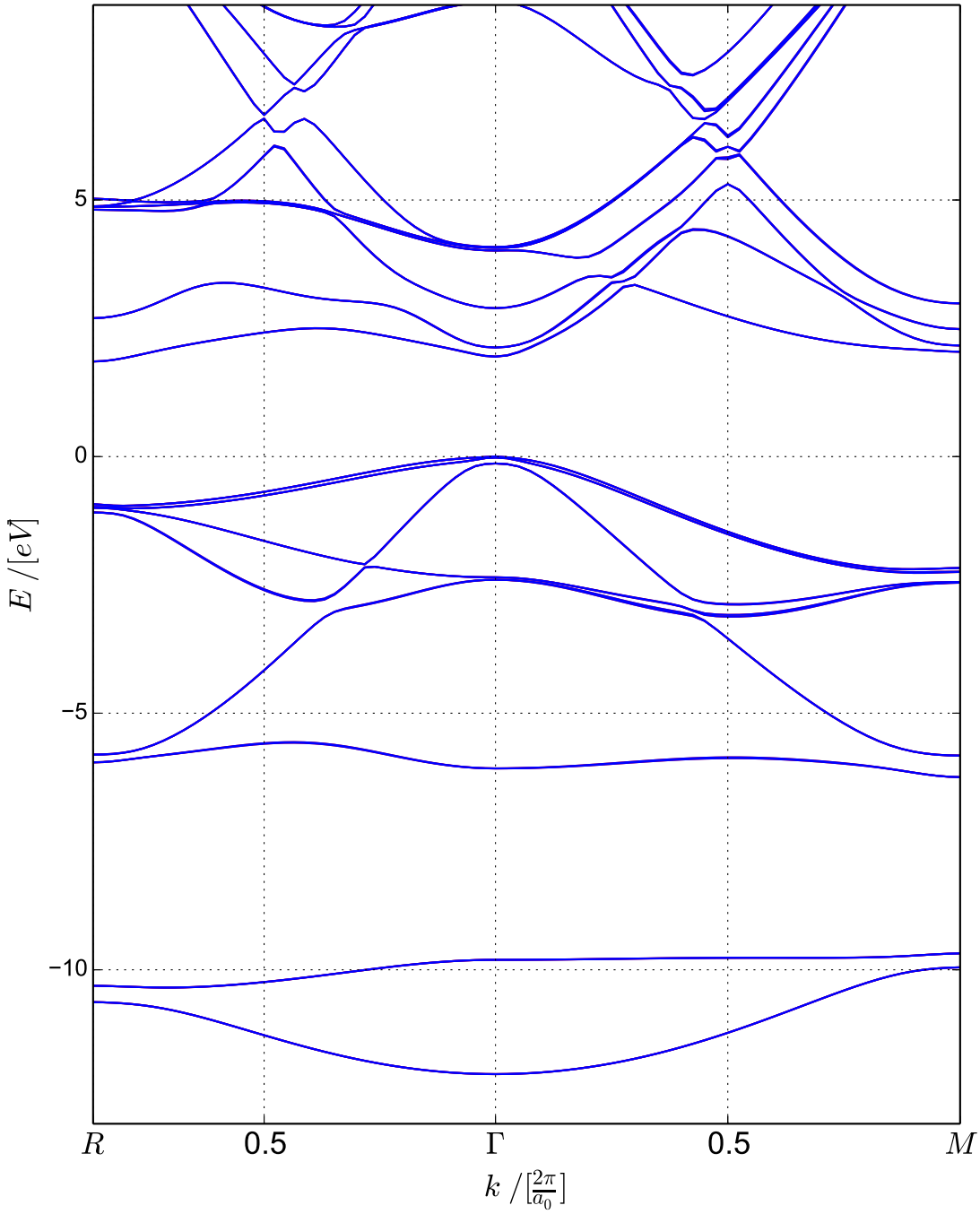

Figure 6.9: The EPM bandstructure of $(GaAs)_1/(AlAs)_1$ (001) superlattice plotted from $R[\frac{1}{2},\frac{1}{2},\frac{1}{2}]$ to $\Gamma[0,0,0]$ and then to $M[1,0,0]$. The bands have been scaled to have the zero in energy at the maximum of the upper-most valence band.

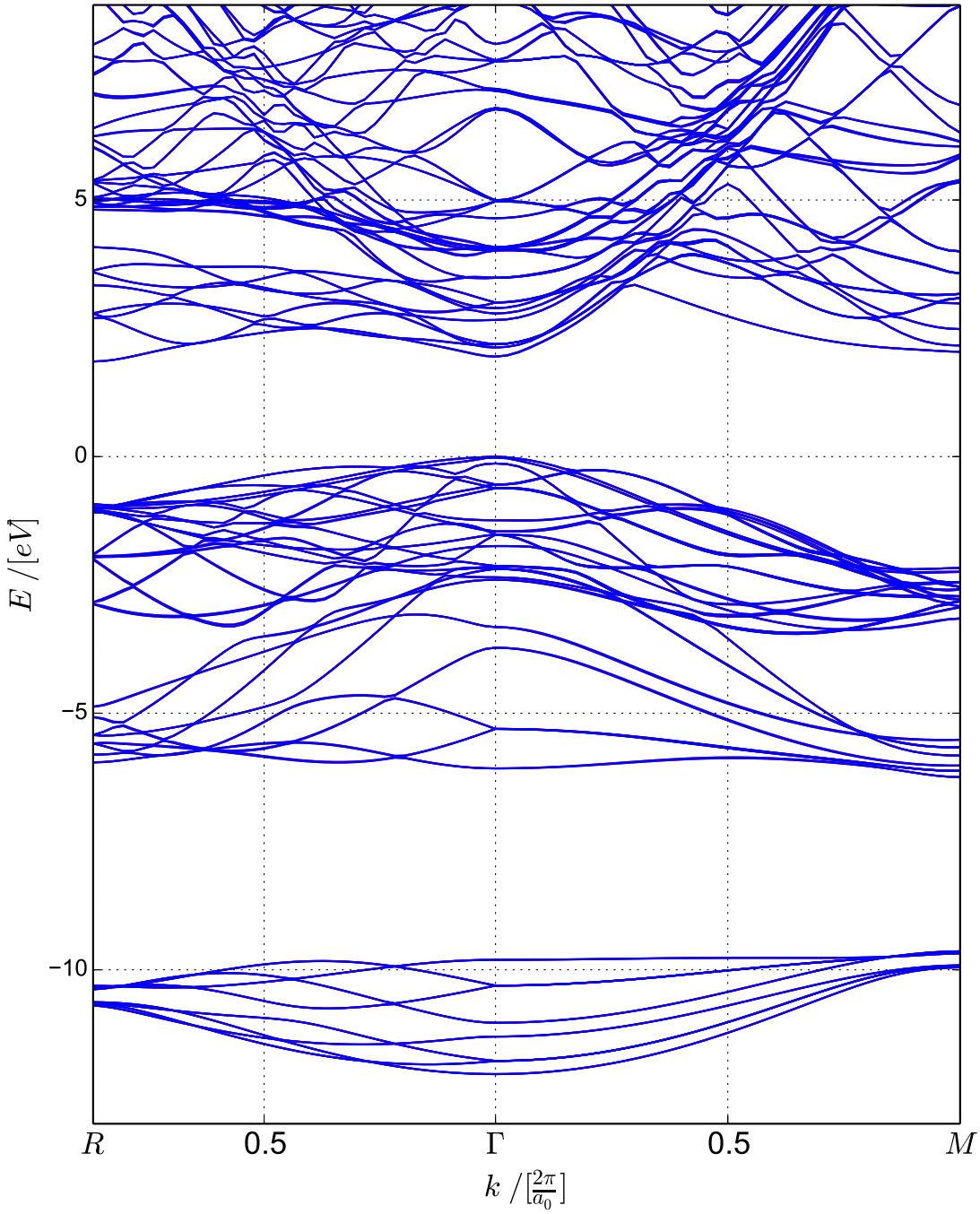

Figure 6.10: EPM bandstructure of $(GaAs)_4/(AlAs)_4$ (001) superlattice plotted from $R[\frac{1}{2},\frac{1}{2},\frac{1}{2}]$ to $\Gamma[0,0,0]$ and then to $M[1,0,0]$. The bands have been scaled to have the zero in energy at the maximum of the upper-most valence band

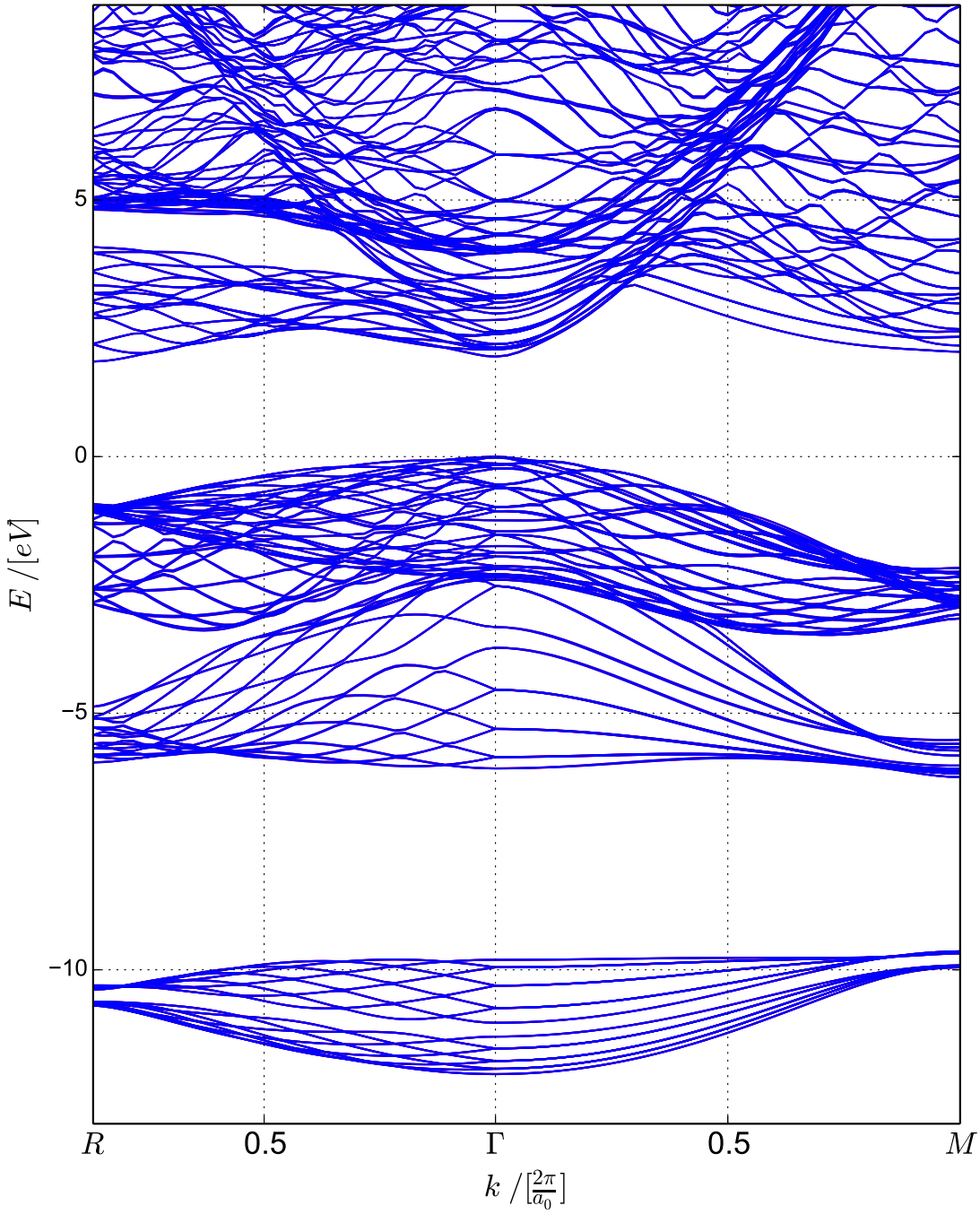

Figure 6.11: EPM bandstructure of $(GaAs)_8/(AlAs)_8$ (001) superlattice plotted from $R[\frac{1}{2},\frac{1}{2},\frac{1}{2}]$ to $\Gamma[0,0,0]$ and then to $M[1,0,0]$. The bands have been scaled to have the zero in energy at the maximum of the upper-most valence band

Chapter 7

Conclusion

7.1 Summary and discussion

The seminal paper by Mäder and Zunger[3] introduced the idea of using a linear combination of Gaussians in the EPM to interpolate the atomic form factor potentials. Although this idea has been used extensively -indeed their paper has to date being cited more than 1200 times- we have seen that there is in fact no particular advantage in using this interpolation when it comes for fitting the bandstructures by optimization. In the present study the Levernberg-Marquardt algorithm was used to obtain optimized cubic spline interpolations of the atomic form factor potentials. It was illustrated that due to the piecewise nature of the cubic spline interpolations, a more rapid convergence towards the optimal fit could be obtained for the same number of independent coefficients. Since in the case of superlattice the bandstructure calculation, according to the EPM, can be computationally demanding even on the best computers today, the rate of convergence is an important consideration when trying to optimize form factors by directly comparing the energy band structure of layered semiconductor systems.

A substantial part of this study involved developing the necessary codes, firstly to implement the basic EPM within the large basis approach and, secondly to incorporate these

codes into Levenberg-Marquardt algorithm. Before we proceed to calculate the bandstructures of layered semiconductor material, we first calculated the bandstructure for bulk semiconductor material. The fact that for bulk material, only the knowledge of the atomic form factor potential at the discrete points of q is enough for bandstructure calculations was confirmed. The reliability of the optimized cubic spline atomic form factor potentials calculated in this work, is illustrated through the energy band gaps measured in layered structures.

7.2 Out look for future work

Indeed the results obtained in this work are satisfactory, but there is still room for improvement. In future we plan to optimize the cubic spline atomic form factor potentials by calculating a residual between layered structures calculated with other methods. Layered structure calculations can be at computationally demanding incorporating other computational techniques such as parallization can assist in optimizing computational demands that comes with such systems. We also plan to include an average C atomic form factor potential when calculating a superlattice the form AC/BC as suggested in Ref. [3].

Bibliography

[1] M. Silver, Ph.D. thesis, University of Western Ontario, London Ontario, 1991.

[2] L. Esaki and R. Tsu, IBM J. Res. Dev. **14**, 61 (1970).

[3] Kurt A. Mäder and Alex Zunger, Phys. Rev. B **50**, 17393 (1994).

[4] A. J. Williamson and A. Zunger, Phys. Rev. B **59**, 15819 (1999).

[5] M. M. Rieger and P. Vogl, Phy. Rev. B **48**, 14276 (1993).

[6] P. Friedel, M.S. Hybertsen, and M. Schlüter, Phys. Rev. B **39**, 7974 (1989).

[7] P. B. Allen and M. Cardona, Phys. Rev. B **23**, 1495 (1981).

[8] M. V. Fischetti and S. E. Laux, J. Appl. Phys. **80**, 2234 (1996).

[9] O. J. Glembocki and F. H. Pollak, Phys. Rev. B **25**, 7863 (1982).

[10] C. Y. Yeh, S.B. Zhang, and A. Zunger, Phys. Rev B **50**, 14405 (1994).

[11] L.W. Wang and A. Zunger, J. Phys. Chem **98**, 2158 (1994).

[12] S. B. Zhang, Chin-Yu Yeh, and A. Zunger, Phys. Rev. B **48**, 11204 (1993).

[13] S. Bednarek and U. Rössler, Phys. Rev. Lett. **48**, 1296 (1982).

[14] M. L. Cohen and T. K. Bergstresser, Phys. Rev. **141**, 789 (1966).

[15] J. Kim, Ph.D. thesis, University of Massachusetts, Amherst, USA, 2011.

[16] Marvin L. Cohen and James R. Chelikowsky, *Solid-State Sciences 75*, 1st ed. (Springer-Verlag Berlin Heidelberg, New york, 1988).

[17] James R. Chelikowsky and Marvin L. Cohen, Phys. Rev. B **14**, 556 (1976).

[18] Lin-Wang Wang and Alex Zunger, J. Phys. Chem **98**, 2158 (1993).

[19] E. O. Kane, J. Phys. Chem. Solids **1**, 82 (1956).

[20] E. O. Kane, J. Phys. Chem. Solids **1**, 249 (1957).

[21] L. C. Lew Yan Voon and M. Willatzen, *The kp Method* (Spinger, New York, 2009).

[22] W. Kohn and L. J. Sham, Phys. Rev. A **140**, 1133 (1965).

[23] L.-W. Wang, S.-H. Wei, T. Mattila, A. Zungerand I. Vurgaftman, and J. R. Meyer, Phys. Rev. B **60**, 5590 (1999).

[24] O. Stier, M. Grundmann, and D. Bimberg, Phys. Rev. B **59**, 5688 (1999).

[25] A. E. Botha and M. R. Singh, Phys. Rev. B **67**, 195334 (2003).

[26] S. B. Radhia, N. Fraj, I. Saïdi, and K. Boujdaria, Semicond. Sci. Technol. **22**, 427 (2007).

[27] M. Cardona and F. H. Pollak, Phys. Rev. B **142**, 530 (1965).

[28] I. Saïdi, S. B. Radhia, and K. Boujdaria, J. Appl. Phys. **107**, 043701 (2010).

[29] S. Botti, Ph.D. thesis, Universitá degli studi diPavia, Pavia, 2002.

[30] M. S. Hybertsen and S. G. Louie, Phys. Rev. B **32**, 7005 (1985).

[31] M. S. Hybertsen and S. G. Louie, Phys. Rev. Lett **55**, 1418 (1985).

[32] M. S. Hybertsen and S. G. Louie, Phys. Rev. B **34**, 5390 (1986).

[33] R. W. Godby and M. Schlüter, Phys. Rev. Lett **56**, 2415 (1986).

[34] R. W. Godby, M. Schlüter, and L.J. Sham, Phys. Rev. B **37**, 10159 (1988).

[35] A. J. Cohen, P. Mori-Sánchez, and W. Yang, Science **321**, 792 (2008).

[36] J. P. Perdew, Phys. Rev. Lett **51**, 1884 (1983).

[37] Wei-Feng Sung, Mei-Cheng Li, and Lian-Cheng Zhao, Superlattices and Microstructures **49**, 81 (2011).

[38] L. H. Thomas, Proc. Cambridge Phil. Roy. Soc. **23**, 542 (1927).

[39] P. A. M. Dirac, Proc. Cambridge Phil. Roy. Soc. **26**, 376 (1930).

[40] P. Hohenberg and W. Kohn, Phys. Rev. B **136**, 871 (1965).

[41] P. Y. Yu and M. Cardona, *Fundamentals of Semiconductors: physics and material properties*, 3rd ed. (Springer, New York, 2001).

[42] Antoni Rogalski, J. of All. and Comp. **371**, 53 (2004).

[43] A. Rogalski and P. Martyniuk, Infr. Phys. and Tech. **48**, 39 (2004).

[44] Herbert Kroemer, Physica E **20**, 196 (2004).

[45] T. Yao, Appl. Phys. Lett. **51**, 1798 (1994).

[46] G. A. Sai-Halasz, L. Esaki, and W. A. Harrison, Phys. Rev. B **18**, 2812 (1978).

[47] G. Chen, J. Heat Transfer **119**, 220 (1997).

[48] D. L. Smith and C. Mailhiot, Reviews of Mordern Physics **62**, 173 (1990).

[49] E. D. Caruthers and P.J. Lin-Chung, Phys. Rev. lett **38**, 26 (1976).

[50] E. D. Caruthers and P.J. Lin-Chung, J. Vac. Sci. Technol **15**, 1459 (1978).

[51] W. Andreoni and R. Car, Phys. Rev. B **21**, 3334 (1980).

[52] G. Dresselhaus, Phys. Rev. **100**, 580 (1955).

[53] Z. Chen, S. N. Mohammad, and H. Morkoc, Phy. Rev. B **53**, 3879 (1996).

[54] Paul Harrison, *Quantum Wells, Wires and Dots*, 2nd ed. (Wiley, New York, 2005).

[55] J. M. Luttinger and W. Kohn, Phys. Rev. **97**, 869 (1955).

[56] C. K. Pidgeon and R. N. Brown, Phys. Rev. **146**, 575 (1966).

[57] M. Cardona, N. E. Christensen, and G. Fasol, Phys. Rev. B **38**, 1806 (1988).

[58] D. M. Wood and A. Zunger, Phys. Rev. B **53**, 7949 (1996).

[59] R. Winkler and U. Rössler, Phys. Rev. B **48**, 8918 (1993).

[60] R. Martin, *Electronic Structures* (Cambridge, London, 2005).

[61] J. C. Phillips, Phys. Rev. **112**, 685 (1958).

[62] J. C. Phillips and L. Kleinman, Phys. Rev. **116**, 287 (1959).

[63] L. Kleinman and J. C. Phillips, Phys. Rev. **118**, 1153 (1960).

[64] S. Bloom and T. K. Bergstresser, Solid State Commum. **6**, 465 (1966).

[65] G. Weisz, Phys. Rev **149**, 504 (1966).

[66] J. P. Walter, M. L. Cohen, Y. Petroff, and M. Balkanski, Phys. Rev. B **1**, 2661 (1970).

[67] O. Madelung, *Landolt-Bornstein: Numerical Data and Functional Relationships in Science and Technology* (Springer-Verlag, Berlin, 1982).

[68] N. Bouarissa, Phys. Lett. A **245**, 285 (1998).

[69] M. Goano, E. Bellotti, E. Ghillino, C. Garetto, G. Ghione, and K. F. Brennan, Journal of Applied Physics **88**, 6476 (2000).

[70] K. Kassali. and N. Bouarissa, Solid State Electronics Chem. Solids **44**, 501 (2000).

[71] F. Long, P. Harrison, and W. E. Hagston, J. Appl. Phys. **79**, 6939 (1996).

[72] F. Oyafuso, P. Von Allmen, M. Grupen, and K. Hess, VLSI DESIGN **8**, 463 (1998).

[73] R. A. Pollak, L. Ley, S. Kowalcyzk, D. A. Shirley, D. J. Chadi J. Joannopoulos, and M. L. Cohen, Phys. Rev. Lett. **29**, 1103 (1973).

[74] L. Ley, R. A. Pollak, F. R. McFeey, S. P. Kowalckyzk, and D. A. Shirley, Phys. Rev. B **9**, 600 (1974).

[75] W. D. Grobman and D. E. Eastman, Phys. Rev. Lett. **29**, 1508 (1972).

[76] D. E. Eastman, W. D. Grobman, J. L. Freeouf, and M. Erbudak, Phy. Rev. B **9**, 3473 (1974).

[77] K. C. Pandey and J. C. Phillips, Phys. Rev. B **9**, 1552 (1974).

[78] J. C. Phillips and K. C Pandey, Phys. Rev. Lett. **30**, 787 (1973).

[79] James R. Chelikowsky and Marvin L. Cohen, Phys. Rev. Lett. **32**, 674 (1973).

[80] D. Brust, Phys. Rev. B **4**, 3497 (1971).

[81] D. Dugdale, Ph.D. thesis, University of Durham, United Kingdom, Durham, 2000.

[82] H. P. Gavin, Tech. Rep. Duke University 1 (2011).

[83] S. Roweis, Levenberg-Marquardt Optimization. Tech. rep. , Available on line at http://www.cs.nyu.edu/roweis/notes/lm.pdf (2013).

[84] M. Gilli, D. Maringer, and E Schumann, *Numerical Methods and Optimization in Finance* (Academic Press, Waltham, MA, USA, 2011), Vol. 88.

[85] D. Marquardt, SIAM J. Appl. Math. **11**, 431 (1963).

[86] Carl de Boor, *A Practical Guide to Splines* (Springer, New York, 2001).

[87] Kenneth L. Judd, *Numerical Methods in Economics* (MIT Press, United States of America, 1996).

[88] W. Andreoni, A. Baldereschi, and R. Car, Solid State Commun. **27**, 821 (1978).

[89] J. B. Xia, Phys. Rev. B **38**, 8365 (1988).

[90] H. P. Langtangen, *Python Scripting for Computational Science* (Springer Verlag, Berlin, 2004).

[91] T. C. Chiang, J. A. Knapp, M. Aono, and D. E. Eastman, Phys. Rev. B **21**, 3513 (1980).

[92] D. D. Sell, Phys. Rev. B **6**, 3750 (1972).

[93] D. E. Aspen, C. G. Olson, and D. W. Lynch, Phys. Rev. Lett. **37**, 766 (1976).

[94] B. Monemar, Phys. Rev. B **8**, 5711 (1973).

[95] D.J. Wolford and J. A. Bradeley, Solid State Commun **53**, 1069 (1985).

[96] A. Onton, *in Proceedings of the 10th International Conference on the Physics of Semiconductors* (USAEC, New York, 1970), p. 107.

[97] Z. Ikonic, G. P. Srivastava, and J. C. Inkson, Phys. Rev. B **46**, 15150 (1992).

[98] D. Munzar, Phy. Stat. Sol. b **175**, 395 (1993).

[99] R. Eppenga, M. F. H. Schuurmans, and S. Colak, Phys. Rev. B **36**, 1554 (1987).

[100] W. Ge, W. D. Schmidt, M.D. Struge, L. N. Pfeiffer, and K. W. west, J. Lumin. **59**, 163 (1994).